"Explicit Polarization Theory," Y. Wang, M. J. M. Mazack, D. G. Truhlar, and J. Gao,
in *Many-Body Effects and Electrostatics in Biomolecules*, edited by Q. Cui, M. Meuwly, and P. Ren
(CRC Press, Boca Raton, FL, 2016), pp. 33-64

Explicit Polarization Theory

Yingjie Wang,[a] Michael J. M. Mazack,[a] Donald G. Truhlar,[a] and Jiali Gao[a,b]

[a] *Department of Chemistry and Supercomputing Institute, University of Minnesota, Minneapolis, MN 55455, USA*
[b] *Theoretical Chemistry Institute, State Key Laboratory of Theoretical and Computational Chemistry, Jilin University, Changchun, Jilin Province 130023, P. R. China*
jiali@jialigao.org

Molecular mechanical force fields have been successfully used to model condensed-phase and biomolecular systems for a half century. Molecular mechanical force fields are analytic potential energy functions based on classical mechanical force constants, van der Waals potentials, electrostatics, and torsional potentials, with parameters fit to experiment, to quantum mechanical calculations, or to both. Accurate results can be obtained from simulations employing molecular mechanics for processes not involving bond breaking or bond forming. In this chapter, we describe a new approach to developing force fields; this approach involves the direct use of quantum mechanical calculations rather than using them as a training set for classical mechanical force fields. Computational efficiency is achieved by partitioning of the entire system into molecular fragments. Since the mutual electronic polarization is explicitly treated by electronic structural theory, we call this

approach the explicit polarization (X-Pol) method. Strategies and examples are presented to illustrate the application of X-Pol to describe intermolecular interactions as a quantum chemical model and as a force field to carry out statistical mechanical Monte Carlo and molecular dynamics simulations.

2.1 Introduction

Molecular mechanical force fields (MMFFs) were first proposed in the 1940s to study steric effects of organic molecules[1,2] and were extended to model biomolecular systems by Lifson and coworkers in the 1960s.[3–5] Since that time, significant progress has been made, and a number of force fields have been developed that can be used to provide excellent quantitative interpretation of experimental observations.[6–27]

Although the widely used force fields differ in their details (for example, some of them include coupling between internal coordinates), the functional forms used in MMFFs have remained essentially unchanged over the past half century,[5,28] and the functional form depicted in Eq. 2.1 captures the essence of a typical MMFF potential energy function:

$$V = \sum_{b}^{\text{bonds}} \frac{1}{2} K_b (R_b - R_b^o)^2 + \sum_{a}^{\text{angles}} \frac{1}{2} K_a (\theta_a - \theta_a^o)^2 + \sum_{t}^{\text{torsion}} \sum_{n} \frac{V_t^n}{2} [1 + \cos(n\phi_t - \phi_t^o)] + \sum_{i<j} \left\{ \varepsilon_{ij} \left[\left(\frac{\sigma_{ij}}{R_{ij}} \right)^{12} - \left(\frac{\sigma_{ij}}{R_{ij}} \right)^{6} \right] + \frac{q_i q_j}{R_{ij}} \right\} \quad (2.1)$$

In this equation, the first sum accounts for bond stretching, the second sum for valence angle bending, the third (double) sum for torsions, and the fourth, where the sum goes only over nonbonded and nongeminal atoms, for van der Waals interactions and nonbonded Coulomb forces.

The importance of polarization has long been recognized, and Eq. (2.1) includes polarization implicitly through the choice of

parameters, which are often designed to include not just the effect of intramolecular polarization but also the effect of polarization by the solvent or other surroundings in a condensed-phase medium. Major current efforts in improving MMFFs are being devoted to the explicit inclusion of polarization by means of terms of various forms to account for inductive forces.[29–49] We will label force fields that include polarization explicitly as polarized molecular mechanics force fields or PMMFFs, while we restrict the acronym MMFFs to force fields that include polarization only implicitly through the parametrization.

Despite the success of molecular mechanics,[28,50,51] there are also a number of limitations: There is no general approach to treat the coupling of internal degrees freedom, the treatment of electronic polarization is difficult, intermolecular charge transfer is neglected, excited electronic states cannot be treated, and in the form usually employed the methods are inapplicable to chemical reactions.[28] In recent years, some extensions to treat chemically reactive systems have been presented,[52–55] and one can overcome some of the limitations in specific applications by introducing additional empirical terms,[31,32,56,57] but here we discuss another approach, where the whole treatment is intrinsically based on quantum mechanics (QM).

Quantum mechanical electronic structure calculations can provide both reactive and nonreactive potential energy surfaces, including not only electrostatics and van der Waals forces but also polarization and charge transfer effects. However, it is a daunting task (essentially impossible) to solve the Schrödinger equation for a condensed-phase system. Therefore, a wide range of approximate quantum chemical model chemistries have been developed, including both wave function theory (WFT)[58] and density functional theory (DFT),[59] as well as various linear scaling and fragment-based QM methods that have been proposed to reduce the computation costs.[60–95] The latter represents an active approach to balance accuracy and efficiency in applying electronic structural methods to large systems.

The explicit polarization (X-Pol) model is a fragment-based QM method, in which the entire system is divided into molecular subunits,[65,66,77,80] which can be individual molecules, ions, ligands

or cofactors, and amino acid residues or a group of these entities. The key assumption in the X-Pol method is that the wave function of the entire system is approximated as a Hartree product of the wave functions of the individual fragments. Consequently, the optimization of the total wave function can be reduced to the optimization of each fragment embedded in and polarized by the rest of the system. Clearly, variational optimization of the mutual dependence of the fragmental wave functions is critical to the success of this method. As a force field, the energy of each fragment corresponding to the intramolecular energy terms in an MMFF is determined by the electronic structure method used, whereas intermolecular interactions are modeled through electrostatic embedding in terms of one-electron integrals. The short-range exchange repulsion interactions between fragments, the long-range dispersion interactions between different fragments, and the interfragment correlation energy are neglected in the Hartree product approximation but are modeled empirically as in molecular mechanics.[65,66,77] Alternatively, these energy contributions can be modeled by density-dependent functional,[96,97] by Hartree–Fock (HF) exchange,[98] or by making use of many-body expansion corrections.[99] The latter also takes into account interfragment charge transfer effects, which are otherwise neglected, although intrafragment charge transfer is fully included. X-Pol[92] can also be used as a general QM-QM fragment-coupling scheme,[88,100,101] in which different levels of theory are employed to model different fragments; we refer to this as a multilevel method.

In the following sections, we summarize the theoretical formulation of the X-Pol model and illustrate the multilevel X-Pol[92] method for studying intermolecular interactions. In addition, we discuss our work on using X-Pol as a quantum mechanical force field (QMFF) for liquid water simulations.

2.2 Theoretical Background

In X-Pol, a macromolecular system is partitioned into molecular fragments, which may be called monomers. The division is flexible within the constraint that monomers do not overlap, (i.e., the

subsystem included in one fragment does not appear in another monomer). For solutions with small solute molecules, a fragment can be a single solute or solvent molecule.[65,66] For large solute molecules or biomacromolecules, (e.g., a protein or enzyme–substrate complex) a fragment can be a connected group of atoms (e.g., peptide unit, or a metal atom or ion, a cofactor, or a substrate molecule).[77,102] Several peptide units can be combined into the same fragment, if desired, which can be useful for modeling systems containing disulfide bonds. The X-Pol method is derived from a standard electronic structure method by a nested set of three approximations, described next.

2.2.1 *Approximation of the Total Wave Function and Total Energy*

The first approximation in the X-Pol theory is that the molecular wave function of the entire system Ψ is approximated as a Hartree product of the antisymmetric wave functions of individual fragments, $\{\Psi_A; A = 1, \cdots, N\}$:

$$\Psi = \prod_{A=1}^{N} \Psi_A. \tag{2.2}$$

The wave function of fragment A, Ψ_A, can either be a single determinant from HF theory or Kohn–Sham DFT, or a multiconfiguration wave function derived from complete active space self-consistent field (CASSCF) or valence bond (VB) calculations.

The effective Hamiltonian of the system is expressed as Eq. 2.3

$$\hat{H} = \sum_{A}^{N} \hat{H}_A^o + \frac{1}{2}\sum_{A}^{N}\sum_{B\neq A}^{N}(\hat{H}_A^{int}[\rho_B] + E_{AB}^{XD}), \tag{2.3}$$

where the first term sums over the Hamiltonians of all isolated fragments and the second double summation accounts for pairwise interactions among all the fragments. The explicit form of $\hat{H}_A^o$, which is the Hamiltonian for an isolated fragment A in the gas phase, varies according to the level of theory employed, for instance, post-HF correlated methods can be used to treat the active site of an enzyme, and HF or semiempirical molecular orbital methods can be used to treat solvent molecules or peptide units that are distant from the

reactive center. The Hamiltonian $\hat{H}_A^{int}[\rho_B]$ represents electrostatic interactions between fragments A and B, and the final term E_{AB}^{XD} specifies exchange-repulsion, dispersion and other interfragment correlation energy contributions, and charge transfer interactions, as explained in more detail in the following sections.

The total energy of the system is written as the expectation value of the effective Hamiltonian,

$$E[\{\rho\}] = <\Psi|H|\Psi> \; = \sum_A^N E_A + \frac{1}{2}\sum_A^N \sum_{B\neq A}^N (E_{AB}^{int}[\rho_A, \rho_B] + E_{AB}^{XD}) \tag{2.4}$$

where E_A is the energy of fragment A that is determined using its wave function as *polarized* by all other fragments, and $E_{AB}^{int}[\rho_A, \rho_B]$ is the electrostatic interaction energy between fragments A and B, again calculated using the polarized wave functions. The latter term is calculated from the point of view of fragment A and also from the point of view of fragment B, and the sum of these results is divided by two since the same interactions are counted twice. Therefore, we have

$$E_A = <\Psi_A|\hat{H}_A^0|\Psi_A>, \tag{2.5}$$

$$E_{AB}^{int}[\rho_A, \rho_B] = \frac{1}{2}\left(<\Psi_A|\hat{H}_A^{int}[\rho_B]|\Psi_A> + <\Psi_B|\hat{H}_B^{int}[\rho_A]|\Psi_B>\right). \tag{2.6}$$

2.2.2 *Approximation on the Electrostatic Interaction between Fragments*

The second approximation in the X-Pol theory is the method of treating the interaction between fragments. The interaction Hamiltonian between fragment A and B is defined as

$$\hat{H}_A^{int}[\rho_B] = -\sum_{i=1}^{M_A} e\,\Phi_E^B(\mathbf{r}_i^A) + \sum_{\alpha=1}^{N_A} Z_\alpha^A \Phi_E^B(\mathbf{R}_\alpha^A), \tag{2.7}$$

where M_A and N_A are respectively the number of electrons and nuclei in fragment A, Z_α^A is the nuclear charge of atom α of fragment A, and $\Phi_E^B(\mathbf{r}_x^A)$ is the electrostatic potential at $\mathbf{r}_x$ from fragment B. The electrostatic potential is given by

$$\Phi_E^B(\mathbf{r}_x^A) = \int \frac{\rho_B(\mathbf{r}')}{|\mathbf{r}_x^A - \mathbf{r}'|} d\mathbf{r}', \tag{2.8}$$

where $\rho_B(\mathbf{r}') = -\rho_{ele}^B(\mathbf{r}') + \sum_\beta Z_\beta^B \delta(\mathbf{r}' - \mathbf{R}_\beta^B)$ is the total charge density of fragment B, including electron density $\rho_{ele}^B(\mathbf{r}')$ and nuclear charge Z_β^B at $\mathbf{R}_\beta^B$. The potential $\Phi_E^B(\mathbf{r}_x^A)$ can be used directly to determine the electrostatic interaction energy of Eq. 2.7; this involves or is equivalent to evaluating the corresponding four-index two-electron integrals explicitly, which is time-consuming and could be ill-behaved when large basis sets are used. Although it yields the classical electrostatic part of the interaction without approximation, it does not include the exchange repulsion part of the interfragment interaction or the interfragment correlation energy, which will be discussed in Section 2.2.3. To reduce the computational cost in two-electron integral calculation, it is desirable to an efficient approach to treat interfragment electrostatic interactions.[65,66]

The quantity $\Phi_E^B(\mathbf{r}_x^A)$ may be considered as an embedding potential of fragment A due to the external charge distribution of fragment B, and a number of well-established techniques.[15,21,103–107] can be used to model it. A general approach for the classical electrostatic potential is to use a multicenter multipole expansion,[107] of which the simplest form is to limit the expansion to the monopole terms, so the result only depends on the partial atomic charges. The use of partial atomic charges to approximate $\Phi_E^B(\mathbf{r}_x^A)$ is particularly convenient for constructing the effective Hamiltonian of Eq. 2.7, and this is the strategy that has been adopted for the classical electrostatic part in the X-Pol method.[65,66]

The next issue in modeling the electrostatic interaction is the method to obtain the monopole charges. For these charges, one may use partial atomic charges fitted to the electrostatic potential (ESP)[15,105,106 108–113] or one may use Mulliken population analysis,[104] population analysis based on Löwdin orthogonalization,[103] or class IV charges from mapping procedures[114,115] in which the mapping function has been parametrized to yield atomic charges that reproduce experimental molecular dipole moments. Another method is based on optimization of atomic charges to reproduce the molecular multipole moments from QM calculations, and we have recently used a procedure that preserves the molecular dipole moment and polarizability to generate dipole-preserving and polarization-consistent charges (DPPCs).[116]

Using the approximation of point charges, Eq. 2.8 is simplified to

$$\Phi_{\mathrm{E}}^{B}(\mathbf{r}_x^A) = \sum_{\beta} \frac{q_\beta^B}{|\mathbf{r}_x^A - \mathbf{R}_\beta^B|}. \tag{2.9}$$

2.2.3 *Approximations to Interfragment Exchange–Dispersion Interactions*

The Hartree product wave function in Eq. 2.2 neglects the long-range interfragment dispersion interactions, the other interfragment correlation energy contributions, and the short-range interfragment exchange-repulsion interactions arising from the Pauli exclusion principle. Furthermore, the partition of a molecular system into fragments and the restriction to an integer number of electrons in each fragment precludes charge transfer between the fragments. But interfragment dispersion interactions, the other interfragment correlation energy contributions, the short-range exchange-repulsion interactions, and charge transfer make critical contributions to intermolecular interactions, so they must be added to the X-Pol energy expression. A brute force approach is to employ variational many-body expansion (VMB) theory to make two-body, three-body, and higher order corrections.[99] Although the accuracy can be systematically improved by using many-body corrections, the number of terms involved increases rapidly with the number of fragments and the order of correction, rendering this approach impractical beyond two-body correction terms. Thus in using this approach, it is critical to define the reference state for the monomer energies such that the higher-order correction terms are negligible. However, when the X-Pol method is used as a theoretical framework to develop force fields for condensed-phase and macromolecular systems, we can use a simpler approach. In particular, we introduce empirical terms such as Lennard-Jones or Buckingham potentials (as used in molecular mechanics) to estimate the exchange repulsion, dispersion, other interfragment correlation, and charge transfer energies. In one of the applications described in Section 2.4.1,[92] we add the following pairwise Buckingham-potential term to the interaction energy between fragments A and B:

$$E_{AB}^{\mathrm{XD}} = \sum_{I}^{N_A} \sum_{J}^{N_B} \left(A_{IJ} e^{-B_{IJ} \cdot R_{IJ}} - \frac{C_{IJ}}{R_{IJ}^6} \right) \tag{2.10}$$

where the parameters are determined from the atomic parameters according to combining rules:

$$A_{IJ} = (A_I A_J)^{1/2} \tag{2.11}$$

$$B_{IJ} = (B_I + B_J)/2 \tag{2.12}$$

$$C_{IJ} = (C_I C_J)^{1/2} \tag{2.13}$$

In the other application discussed in Section 2.4.2, we used pairwise Lennard-Jones potentials.

2.2.4 *Double Self-Consistent Field*

As in standard electronic structure methods, the Roothaan–Hall equation on each fragment in X-Pol is solved iteratively. However, in X-Pol, in addition to the SCF convergence within each molecular fragment, the mutual polarization among all fragments of the whole system must be converged. A procedure is depicted in Fig. 2.1, which may be described as a double self-consistent field (DSCF) iterative scheme. In practice, however, there is no need to fully converge the inner, intrafragment SCF before proceeding to the next iteration step for the outer, interfragment SCF. We found that it is often computationally efficient to carry out two to three iterations in the intrafragment SCF between the outer SCF iterations.

There are two ways of constructing the Fock matrix for solving the DSCF equations; one is based on the variational optimization of the energy of Eq. 2.4,[80] and the other, which was first used in Monte Carlo simulations where analytic forces are not required,[65,66] is written by assuming that each monomer is embedded in the fixed electrostatic field of the rest of the system. The two approaches are discussed next.

(a) Variational X-Pol. In X-Pol, the Fock operator for a fragment, A, is derived by taking the derivative of the total energy (Eq. 2.4) with

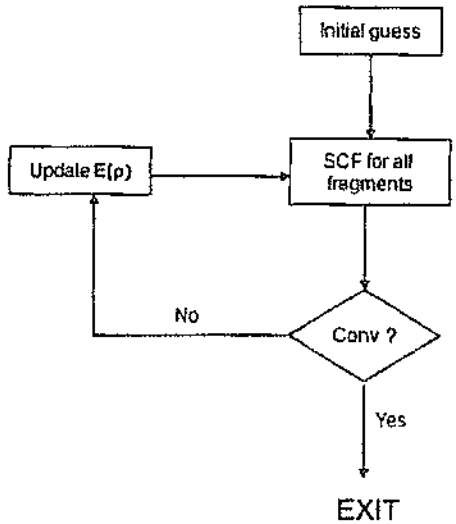

Figure 2.1 The schematic flow chart of DSCF iterations.

respect to each element $P^A_{\mu\nu}$ of the electron density matrix:

$$\mathbf{F}^{A,\mathrm{Xpol}}_{\mu\nu} = \frac{\partial E[\{\rho\}]}{\partial P^{A,SCF}_{\mu\nu}} = \mathbf{F}^{A,o}_{\mu\nu} - \frac{1}{2}\sum_{B\neq A}\sum_{b\in B} q^B_b \left(\mathbf{I}^B_b\right)^A_{\mu\nu} - \frac{1}{2}\sum_{a\in A} X^A_a \left(\Lambda^A_a\right)_{\mu\nu}, \tag{2.14}$$

where $\mathbf{F}^{A,o}_{\mu\nu}$ is the Fock matrix element for the Hamiltonian of the isolated fragment A, q^B_b is the point charge on atom b of fragment B, $\mathbf{I}^B_b$ is the matrix of the one-electron integrals of the embedding potential due to fragment B, X^A_a is a vector arising from the derivative of the electrostatic interaction energy with respect to the point charge of atom a:

$$X^A_a = \sum_{B\neq A}\left(\sum_{\lambda\sigma} P^B_{\lambda\sigma}\left(\mathbf{I}^A_a\right)^B_{\lambda\sigma} + \sum_{b\in B}\frac{Z^B_b}{|\mathbf{R}^B_b - \mathbf{R}^A_a|}\right), \tag{2.15}$$

and Λ^A_a is the response density matrix:

$$\left(\Lambda^A_a\right)_{\mu\nu} = \frac{\partial q^A_a}{\partial P^{A,\mathrm{SCF}}_{\mu\nu}} = \frac{\partial q^{A,\mathrm{SCF}}_a}{\partial P^{A,\mathrm{SCF}}_{\mu\nu}}. \tag{2.16}$$

(b) Charge-embedding X-Pol. If each fragment is considered to be embedded in the instantaneous static electrostatic field of the rest of the system, one can construct a Fock operator for fragment A simply as follows:

$$\mathbf{F}^{A,CE} = \mathbf{F}^{A,o} - \sum_{B\neq A}\sum_{b\in B} q^B_b \left(\mathbf{I}^B_b\right)^A. \tag{2.17}$$

In the charge-embedding approach, the mutual polarization among all fragments in the system is achieved by iteratively updating the partial atomic charges $\{q^B_b\}$ derived from the wave function for each fragment in each outer, interfragment SCF step (Fig. 2.1). Note that Eq. 2.14 indicates that the wave function of each fragment, A, is fully polarized by the full electric field of all other fragments, but the total interaction energy will be determined by multiplying a factor of 0.5 since the interactions between two monomers are counted twice. Similar expressions are often found in continuum self-consistent reaction field models for solvation.

Comparison. In comparing methods a and b, we note that the variational X-Pol method has the advantage of allowing the computation of analytic gradients for efficient geometry optimization and dynamics simulations. Furthermore, the total energy obtained from the variational procedure is necessarily lower than that from the charge-embedding scheme. Consequently, it is expected that the use of the variational X-Pol energy as the monomer energy reference state in many-body energy expansion be more efficient than other alternatives. Although it is possible to obtain analytic gradients for the non-variational, charge-embedding approaches, it generally involves solution of coupled-perturbed self-consistent field (CPSCF) equations, which is more time consuming. As a referee of this manuscript lucidly pointed out, "often in the fragment quantum chemistry literature, those response terms have simply been ignored, with numerical consequences that have never been investigated."

2.3 Computational Details

The X-Pol method has been implemented in a developmental version of the Gaussian software package (H35).[117] Although a single quantum chemical model can be used to represent all fragments, any of the electronic structure methods available in Gaussian, such as HF, DFT, MP2, CCSD, BD, etc., can be mixed to represent different fragments in a multilevel X-Pol calculation. We have illustrated the multilevel approach in a recent study[92] of two hydrogen-bonded complexes, including (a) acetic acid (fragment A) and water (fragment B), and (b) $H_5O_2^+$ ion (fragment A) and four surrounding water molecules (fragments B, five fragments in total). In that work, the geometries of the complexes and isolated monomers were optimized using the M06 exchange-correlation functional[118] and the MG3S[119] basis set, which was followed by single-point, multilevel X-Pol calculations using the 6-31G(d)[120] basis set.

For condensed-phase and macromolecular simulations, we have written an X-Pol software package using the C++ language, which has been incorporated into NAMD[121] and CHARMM.[27] The X-Pol program can be used with the popular NDDO-based semiempirical Hamiltonians as well as the recently developed polarized molecular orbital (PMO) model.[122,123] Molecular dynamics simulations of liquid water have been carried out using the NAMD/X-Pol interface. In addition, we have used an earlier version of the X-Pol model in Monte Carlo simulations of liquid water.

Statistical mechanical Monte Carlo simulations were performed on a system consisting of 267 water molecules in a cubic box, employing the XP3P water model, built upon the PMOw Hamiltonian[124] and the DPPC charge model.[116] Periodic boundary conditions were used along with the isothermal-isobaric ensemble (NPT) at 1 atm and for a temperature ranging from −40 to 100 C. Spherical cutoffs with a switching function between 8.5 Å and 9.0 Å based on oxygen–oxygen separations were employed, and a long-range correction to the Lennard–Jones potential was included. In Monte Carlo simulations, new configurations were generated by randomly translating and rotating a randomly selected water molecule within ranges of ± 0.13 Å and ± 13 . In addition, the volume of the system was changed randomly within the limit of ± 150 Å^3 on every 550th attempted move, and the coordinates of oxygen atoms were scaled accordingly. At least 5×10^6 configurations were discarded for equilibration, followed by an additional 10^7 to 10^8 configurations for averaging. About 6×10^6 configurations can be executed per day on a six-core Intel Xeon X7542 Westmere 2.66 GHz processor.

The XP3P model was further employed in molecular dynamics simulations for 500 ps in the NVT ensemble using the Lowe-Andersen thermostat.[125,126] The volume was fixed at the average value from the Monte Carlo simulation. The monomer geometries were enforced by the SHAKE/RATTLE procedure.[127] The velocity Verlet integration algorithm was used with a 1fs time step. The Monte Carlo simulations were performed using the MCSOL program for X-Pol simulations,[128] while molecular dynamics simulations were carried out using a newly developed X-Pol program[129] written in C++ which has been interfaced both with CHARMM[27] and NAMD.[121]

2.4 Illustrative Examples

2.4.1 *Multilevel X-Pol as a Quantum Chemical Model for Macromolecules*

The X-Pol theory can be used with a combination of different electronic structure methods for different fragments. This provides a general, multi-level QM/QM-type of treatment of a large system, where the region of interest could be modeled by a high-level theory, embedded in an environment modeled by a lower level representation. Some arbitrary combinations of different electronic models are illustrated by calculations[92] of the interaction energy between acetic acid and water at the minimum-energy configuration optimized with M06/MG3S (Fig. 2.2). To represent the electrostatic potential in Eq. 2.9, we used two charge models, Mulliken population analysis (MPA) and ESP charge-fitting with the Merz–Kollman scheme (MK), to construct the charge-embedding Fock matrix (Eq. 2.14), whereas only the MPA charges were used in variational X-Pol (Eq. 2.11).

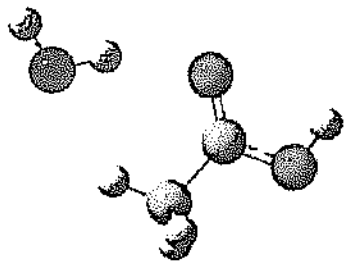

Figure 2.2 Schematic illustration of the optimized configuration of acetic acid and water using M06/MG3S.

The binding energy for a bimolecular complex is defined by

$$\Delta E_b = E_{AB} - E_A^o - E_B^o \tag{2.18}$$

(We have not applied any correction for the basis set superposition error since the main purpose here is to illustrate the possibility of mixing different levels of theory in multi-level X-Pol calculations.) In X-Pol, the binding energy is written as the sum of electrostatic (ΔE_{elec}) and exchange-charge transfer-dispersion (ΔE_{XCD}) terms.

$$\Delta E_b = \Delta E_{\text{elec}} + \Delta E_{\text{XCD}}, \tag{2.19}$$

where the electrostatic interaction energy in X-Pol is given by

$$\Delta E_{\text{elec}} = \frac{1}{2}[E_A^{int}(B) + E_B^{int}(A)] + (E_A - E_A^o) + (E_B - E_B^o), \tag{2.20}$$

where $E_X^{int}(Y)$ represents the interaction of "QM" fragment X polarized by the electrostatic potential from fragment Y, and $(E_X - E_X^o)$ is the energy difference between fragment X in the complex and in isolation. Table 2.1 summarizes the results from these calculations.

The ΔE_{XCD} term can be determined by VMB expansion. For the bimolecular complex in Fig. 2.2, the two-body correction energy is exact. For condensed-phase and macromolecular systems, it is convenient to simply approximate ΔE_{XCD} by an empirical potential such as the Lennard–Jones potential or the Buckingham potential.

The total binding energy between acetic acid and water were estimated to be −6.9 and −6.6 kcal/mol from M06/MG3S and CCSD(T)/MG3S, respectively. Therefore, Table 2.1 shows that the

Table 2.1 Computed electrostatic interactions energies ΔE_{elec} (kcal/mol) between acetic acid (A) and water (B) using multilevel X-Pol with the charge-embedding and variational interaction Hamiltonians

A	B	Charge-embedding		Variational	Full QM[a]
		MK-ESP	MPA	MPA	
M06	M06	−7.0	−7.7	−9.0	−6.9
M06	B3LYP	−6.8	7.3	−8.7	−6.9
M06	HF	−7.2	7.9	9.4	−6.9
MP2	HF	−7.1	−7.7	−8.0	−6.5
CCSD	M06	−7.2	7.6	−8.0	−6.6[b]

Note: The 6-31G(d) basis set was used in all calculations with the M06/MG3S optimized monomer and dimer geometries.
[a]Computed for the complex using the method listed under A with the MG3S basis set.
[b]Determined using CCSD(T)

approximate electrostatic components computed by the X-Pol method overestimate binding interactions for all combinations of methods examined except the combination of M06 for acetic acid and B3LYP for water. Within the charge-embedding scheme, the use of ESP-fitted charges resulted in somewhat weaker binding interactions than those from Mulliken population analysis. However, the variational approach yielded binging energies about 1–2 kcal/mol greater than the corresponding embedding model; at the M06/6-31G(d) level, the binding energy difference between the variational X-Pol result and reference value is about 2 kcal/mol. An empirical correction based on the Buckingham potential, dominated by the first term that represent exchange repulsion, gives a correction of 2.1 kcal/mol, and if this is added to the electrostatic terms, the total X-Pol results obtained using the variational approach become more consistent with the values from fully delocalized calculations.

Table 2.2 shows the computed electrostatic interaction energies and the empirical ΔE_{XCD} correction term for a protonated water cluster using the multilevel X-Pol scheme. The protonated water cluster is a Zundel ion $H_5O_2^+$ with four water molecules; the optimized structure of the complex obtained by the M06/MG3S method is illustrated in Fig. 2.3. Next we analyze the individual

Table 2.2 Computed electrostatic interactions energies ΔE_{elec} (kcal/mol) between $H_5O_2^+$ (A) and $(H_2O)_4$ (B) using multilevel X-Pol with the charge-embedding and variational interaction Hamiltonians

A	B	Charge-embedding		Variational		
		MK-ESP	MPA	MPA	ΔE_{XCD}	ΔE_b
M06	M06	−89.1	−87.5	−91.0	18.2	−72.8
M06	B3LYP	−87.7	−85.2	−88.1	18.2	−69.9
M06	HF	−92.0	−91.7	−94.5	18.2	−76.3
MP2	HF	−92.9	−92.7	−94.4	18.2	−76.2
CCSD	M06	−89.5	−88.0	−83.9	18.2	−65.7

Note: The 6-31G(d) basis set was used in all calculations with M06/MG3S optimized monomer and dimer geometries.

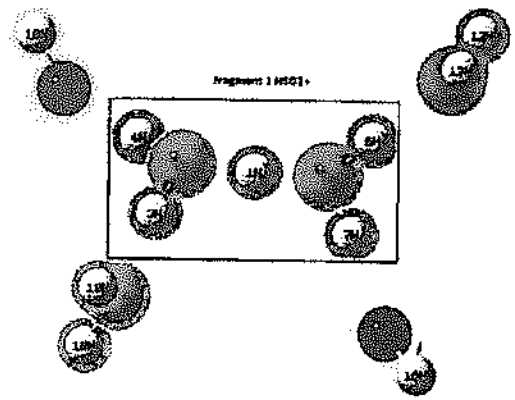

Figure 2.3 Fragment partition of the $H_5O_2^+(H_2O)_4$ cluster optimized using M06/MG3S.

contributions from exchange-repulsion, dispersion and charge transfer interactions.

As explained elsewhere,[98] exchange repulsion can be obtained as the difference between the energy from the antisymmetrized X-Pol wave function for the two fragments, $\hat{A}\{\Psi_A\Psi_B\}$, and the X-Pol electrostatic interaction energy ΔE_{ele} obtained at the SCF level. Using M06/6-31G(d), the charge-embedding scheme yielded an

exchange repulsion energy of 30.0 kcal/mol with the MK charge model and 28.5 kcal/mol with the MPA charge scheme. This may be compared with a value of 35.8 kcal/mol from variational X-Pol using MPA. The difference between the non-variational charge-embedding scheme and the variational X-Pol result shows that there is charge penetration between the two monomer fragments, but the use of unscreened point-charge interactions does not account for this.[130] Note that the exchange energy described above was estimated using the X-Pol electrostatic energy, which is an approximation to the two-electron repulsion integrals between the two fragments, as explained in Section 2.2.2.

The exchange repulsion energy can be obtained more rigorously by block localized energy decomposition analysis,[131,132] and we have carried out this analysis for the complex at the HF/aug-cc-pVDZ level. The computed exchange-repulsion and charge transfer energies are 38.8 kcal/mol and −13.3 kcal/mol, with a net contribution of 25.5 kcal/mol from the two energy terms.

The dispersion-correlation energy can be defined as the difference between the interaction energy computed using an accurate post-Hartree–Fock method and that at the Hartree–Fock level, both corrected by basis set superposition errors. Here, we have not included the BSSE correction contributions, which will affect the quantitative results. Based on the binding energies calculated by CCSD(T)/MG3S (−69.7 kcal/mol) and by HF/aug-cc-pVDZ (−62.4 kcal/mol), we estimate a dispersion-correlation energy of −7.3 kcal/mol. The sum of these terms, that is, 25.5 minus 7.3 kcal/mol, which includes exchange repulsion, charge transfer, and dispersion-correlation, gives an estimate of the ΔE_{XCD} term, which is 18.2 kcal/mol for the interactions between the Zundel ion and four water molecules. Including the ΔE_{XCD} energy, we find that the total X-Pol binding energies from various multilevel calculation range from −65 to −76 kcal/mol, which may be compared with the binding energy computed using CCSD(T)/MG3S (−69.7 kcal/mol) for the full system. The discrepancy between the X-Pol results and full QM results has several contributing factors, chief of which include fixed geometry at a different level of theory and basis set, and the use of a rather small basis set in the X-Pol calculations. Without including ΔE_{XCD}, the binding energies for different X-Pol calculations range

from −83 and −92 kcal/mol, all significantly greater than the full QM value.

2.4.2 *The XP3P Model for Water as a Quantum Mechanical Force Field*

Although ab initio molecular orbital theory and density functional theory can be used to systematically improve the accuracy of X-Pol results for large systems, it is still impractical to use these methods to perform molecular dynamics simulations for an extended period of time. With increased computing power, this will become feasible in the future; however, at present, it is desirable to use semiempirical molecular orbital models such as the popular approaches based on neglect of diatomic differential overlap (NDDO)[133] or the more recent self-consistent-charge tight-binding density functional (SCC-DFTB)[134,135] method to model condensed-phase and biomacromolecules.

Most semiempirical molecular orbital methods are known to be inadequate to describe intermolecular interactions, especially on hydrogen bonding interactions because molecular polarizabilities are systematically underestimated in comparison with experiments. Recently, we introduced a polarized molecular orbital (PMO) method[122–123] which is based on the MNDO[136–138] formalism with the addition of a set of *p*-orbitals on each hydrogen atom.[139] It was found that the computed molecular polarizabilities for a range of compounds containing hydrogen, carbon and oxygen are very significantly improved.[122,123] In addition to the enhancement in computed molecular polarizability, a damped dispersion function is included as a post-SCF correction to the electronic energy. In principle, the Lennard–Jones terms originally adopted in the X-Pol method could be used.[66] Here, we added damped dispersion by following the work of, among others, Tang and Toennies in wave function theory[140] and Grimme in density functional theory[141,142] and we used the parameters proposed by Hillier and co-workers in the PM3-D method.[143–145] The inclusion of the damped dispersion terms further improves the description of intermolecular interactions and the performance of PMO on small molecular clusters.

We note one previous model similar in spirit to PMO, namely the semiempirical self-consistent polarization neglect of diatomic differential overlap (SCP-NDDO) method, parametrized to reproduce properties of water clusters by Chang et al.[146] They obtained a good polarizability of water without using *p* functions on hydrogen (i.e., they used the minimal basis set employed in most NDDO calculations), but their model is parametrized only for water. Since a minimal basis set does not have the flexibility to yield an accurate polarizability in ab initio calculations,[139] it is not clear if the SCP-NDDO-type parametrization could be extended to a broader range of molecules.

The construction of a QMFF based on the X-Pol formalism has two components. First, a computationally efficient quantum chemical model is needed to describe the electronic structure of individual molecular fragments. For liquid water, we adopted the PMOw Hamiltonian,[124] which has been specifically parameterized for compounds containing oxygen and hydrogen atoms. Second, a practical and parametrizable procedure is desired to model interfragment electrostatic and exchange-dispersion interactions. Here, for the electrostatic component, we used the dipole preserving and polarization consistent (DPPC) charges to approximate the electrostatic potential of individual fragments. In this approach, the partial atomic charges are derived to exactly reproduce the instantaneous molecular dipole moment from the polarized electron density of each fragment. Since the DPPC charges are optimized by the Langrangian multiplier technique, there are no adjustable parameters. For the ΔE_{XCD} term, we used pairwise Lennard–Jones potentials, which are based two parameters for each atomic number (with pairwise potentials obtained by combining rules). Employing this strategy, we have developed an X-Pol quantum chemical model for water, called the XP3P model, to be used in fluid simulations.

The computed and experimental thermodynamic and dynamic properties of liquid water at 25 °C and 1 atm are listed in Table 2.3, along with the results from an MMFF, namely TIP3P,[8] and from two PMMFFs, namely AMOEBA[39] and SWM4-NDP.[44] The standard errors ($\pm 1\sigma$) were obtained from fluctuations of separate averages over blocks of 2–4 $\times 10^5$ configurations. The average density of XP3P is 0.996 ± 0.001 g/cm^3 which is within 1% of the experimental value

Table 2.3 Computed liquid properties of the XP3P model for water along with those from experiments, and the TIP3P, AMOEBA, and SWM4-NDP models[a]

	XP3P	TIP3P	AMOEBA	SWM4-NDP	Expt.
ΔH_v, kcal/mol	10.42 ± 0.01	10.41	10.48	10.51	10.51
Density, g/cm^3	0.996 ± 0.001	1.002	1.000	1.000	0.997
C_p, cal mol^{-1} K^{-1}	21.8 ± 1.0	20.0	20.9		18.0
$10^6\kappa$, atm^{-1}	25 ± 2	60			46
$10^5\alpha$, K^{-1}	37 ± 3	75			26
μ_{gas}, D	1.88	2.31	1.77	1.85	1.85
μ_{liq}, D	2.524 ± 0.002	2.31	2.78	2.33	2.3-2.6
$10^5 D$, cm^2/s	2.7	5.1	2.02	2.3	2.3
ε	97 ± 8	92	82	79 ± 3	78

[a] ΔH_v, heat of vaporization; C_p, heat capacity; κ, isothermal compressibility; α, coefficient of thermal expansion, μ, dipole moment; D, diffusion constant; and ε, dielectric constant.

and is similar to results obtained with other polarizable and non-polarizable force fields (see Table 2.3). The heat of vaporization was computed using $\Delta H_v = -E_I(I) + RT$, where $E_I(I)$ is the average interaction energy per monomer from the Monte Carlo simulation, and R and T are the gas constant and temperature. The XP3P model for water yielded an average ΔH_v of 10.42 ± 0.01 kcal/mol using the non-variational (charge-embedding) approximation, whereas the value is increased to 10.58 kcal/mol using the variational Fock operator in molecular dynamics. The variational X-Pol approach lowers the interaction energy in the liquid by about 1.5% as compared to the direct charge-embedding approach. Considering the difficulty to achieve converged results on quantities involving fluctuations, including isothermal compressibility, coefficient of thermal expansion and dielectric constant, overall, the agreement with experiment is good, and the performance of the XP3P model is as good as any other empirical force fields in dynamics simulations.

The average molecular dipole moment of molecules in a condensed phase is not well defined, but it is very common for it to be calculated from partial atomic charges or other analysis methods. We calculated the average dipole moment of water in the liquid $< \mu_{liq} >$ to be 2.524 ± 0.002 D, which represents an increase of 35% relative to the gasphase equilibrium-geometry value (1.88 D

from the PMOw Hamiltonian). We found that water molecules in the liquid experience a wide spectrum of instantaneous electrostatic fields from the rest of the system, reflected in the distribution of the instantaneous molecular dipole moments that range from 2.1 to 2.9 D. In MMFF models, the dipole moment is fixed and thus has no fluctuation at all. Of the two PMMFFs in the table, the AMOEBA model produced a much larger dipole moment (2.78 D) than PMOw in the liquid, but the SWM4-NDP model yielded a somewhat small value of 2.46 D. The PMMFF model of Dang and Chang[34] increases the dipole moment from an equilibrium value of 1.81 D in the gas to an average value of 2.75 D in the liquid, and a survey of eight PMMFFs by Chen et al.[35] found average dipole moments in the liquid ranging from 2.31 to 2.83 D. Examining two other PMMFFs, Habershon et al.[147] found average dipole moments of 2.35 and 2.46 D. Stern and Berne,[148] based on a fluctuating charge model type of PMMFF, calculated an equilibrium gas-phase dipole moment of 1.86 D, an average gas-phase dipole moment of 1.92 D (3.6% larger than experiment), and a liquid-phase average dipole moment of 3.01 D. With another PMMFF, Yu and van Gunsteren[42] calculated an equilibrium gas-phase dipole moment of 1.86 D and a liquid-phase average dipole moment of 2.57 D.

Murdachaew et al.[149] used the SCP-NDDO semiempirical molecular orbital model to calculate an increase in the dipole moment from the equilibrium gas-phase value to the liquid-phase value from 2.16 D to 2.8 D, an increase of 30%, whereas with the older PM3[150] and PM6[151] NDDO-type method, which significantly underestimate the polarizability of water, they found that the increase was only 9% and 11%, respectively.

Direct dynamics calculations[152] with the BLYP exchange-correlation functional and electric properties computed from localized Wannier functions predicted an increase of the dipole moment from an equilibrium value of 1.87 D in the gas to an average value of 2.95 D in the liquid.

There is no experimental data for direct comparison, but values ranging from 2.3 to 3.0 D have been advocated, based in part on an estimate for ice Ih.[153,154] The point of these various comparisons of the calculated dipole moment of water in the bulk is not

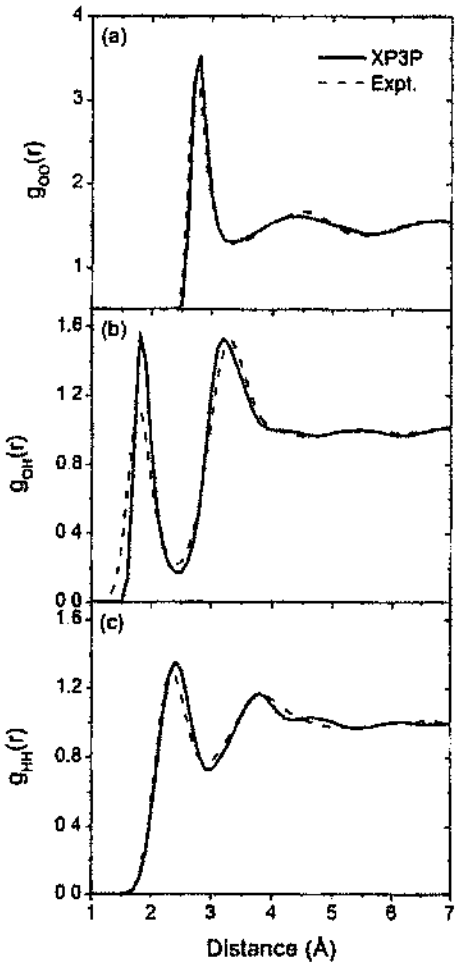

Figure 2.4 Computed (solid) and experimental (dashed) radial distribution functions for O–O, O–H, and H–H pairs in liquid water at 25 °C.

to claim that the X-Pol value is more accurate than the others, but rather to show that it is consistent with the range of previous estimates. Nevertheless, based on analysis of dielectric screening effects of water, Sprik pointed out that an average dipole moment of 2.5–2.6 D in liquid water would most likely yield the correct dielectric constant,[155] and a similar approach was used by Lamoureux et al.[156]

All other thermodynamic and dynamic properties determined using the XP3P model in Table 2.3 are in reasonable accord with experiments and are of similar accuracy in comparison with other empirical models. We note that in contrast to the large number of PMMFFs in the literature that are based on parameterization using different physical approximations, the electronic polarization from the present XP3P model is explicitly described based on a quantum chemical formalism.

Figure 2.4 shows the structure of liquid water characterized by radial distribution functions (RDFs); $g_{xy}(r)$ gives the probability of finding an atom of type y at a distance r from an atom of type x relative to the bulk distribution, where the type is determined by the atomic number. In comparison with the neutron scattering data, the computational results are in excellent agreement with experiments. In particular, a well-resolved minimum following the first peak in the O–O distribution was obtained, whereas the widely used TIP3P and SPC models do not show this feature.[8] For the XP3P potential, the location of the maximum of the first peak of the O-O RDF is 2.78 ± 0.05 Å with a peak height of 3.0. For comparison, the corresponding experimental values are 2.73 Å and 2.8 from neutron diffraction.[157,158] The coordination number of a water molecule in the first solvation layer was estimated to be 4.5, in agreement with the neutron diffraction result of 4.51.[157,158] The oxygen–hydrogen and hydrogen–hydrogen radial distribution functions also agree well with experiments.

2.5 Conclusions

Molecular mechanical force fields (MMFFs) have been successfully used to model condensed-phase and biological systems for a

half century, and more recently polarized molecular mechanics force fields (PMMFFs) have been developed. Thanks to careful parametrization, such classical force fields can be used to provide useful interpretation of experimental findings. In this chapter, we presented a new strategy to construct the potential energy surface for macromolecular systems on the basis of quantum mechanical formalisms. Rather than using quantum chemical results as the target for fitting empirical parameters in the force field, we employ electronic structure theory directly to model intermolecular interactions. As a result, we call this approach a quantum mechanical force field (QMFF).

Our strategy is based on partition of condensed-phase and macromolecular systems into fragments, each of which is explicitly represented by an electronic structure theory with an antisymmetrized wave function. To achieve efficient scaling in the computational cost, the overall molecular wave function of the entire system is approximated by a Hartree product of the individual fragment wave functions. Consequently, the self-consistent field optimization of each molecular wave function can be carried out separately under the influence of the self-consistent polarization by the electric field of the rest of the system. Since the electronic polarization due to interfragment interactions is treated explicitly by electronic structural theory, we call this method the explicit polarization (X-Pol) theory. In this chapter, we summarized the theoretical background of X-Pol and illustrated its application as a versatile electronic structure method to treat intermolecular interactions that can be extended to large molecular and biomolecular systems, including condensed-phase systems. A key application is that we presented an optimized model for statistical mechanical Monte Carlo and molecular dynamics simulations of liquid water by using X-Pol as a QMFF. These illustrative examples in this chapter show that the X-Pol method can be used as a next-generation force field to accurately model molecular complexes and condensed-phase systems and in other work we have also illustrated the method for biomolecular systems.[102]

Acknowledgments

We thank the National Institutes of Health (GM46376) for supporting of this research.

References

1. Hill, T. L. *J. Chem. Phys.* 1946, **14**, 465.
2. Westheimer, F. H. Mayer, J. E. *J. Chem. Phys.* 1946, **14**, 733.
3. Bixon, M. Lifson, S. *Tetrahedron* 1967, **23**, 769.
4. Levitt, M. Lifson, S. *J. Mol. Biol.* 1969, **46**, 269.
5. Levitt, M. *Nat. Struct. Biol.* 2001, **8**, 392.
6. McCammon, J. A. Gelin, B. R. Karplus, M. *Nature* 1977, **267**, 585.
7. Brooks, B. R. Bruccoleri, R. E. Olafson, B. D. States, D. J. Swaminathan, S. Karplus, M. *J. Comput. Chem.* 1983, **4**, 187.
8. Jorgensen, W. L. Chandrasekhar, J. Madura, J. D. Impey, R. W. Klein, M. L. *J. Chem. Phys.* 1983, **79**, 926.
9. Weiner, S. J. Kollman, P. A. Case, D. A. Singh, U. C. Ghio, C. Alagona, G. Profeta, S. Weiner, P. *J. Am. Chem. Soc.* 1984, **106**, 765.
10. Jorgensen, W. L. Tirado-Rives, J. *J. Am. Chem. Soc.* 1988, **110**, 1657.
11. Allinger, N. L. Yuh, Y. H. Lii, J. H. *J. Am. Chem. Soc.* 1989, **111**, 8551.
12. Mayo, S. L. Olafson, B. D. Goddard, W. A. III. *J. Phys. Chem.* 1990, **94**, 8897.
13. Rappé, A. K., Casewit, C. J. Colwell, K. Goddard, W. A. III Skiff, W. *J. Am. Chem. Soc.* 1992, **114**, 10024.
14. Hagler, A. Ewig, C. *Comput. Phys. Commun.* 1994, **84**, 131.
15. Cornell, W. D. Cieplak, P. Bayly, C. I. Gould, I. R. Merz, K. M. Ferguson, D. M. Spellmeyer, D. C. Fox, T. Caldwell, J. W. Kollman, P. A. *J. Am. Chem. Soc.* 1995, **117**, 5179.
16. Halgren, T. A. *J. Comput. Chem.* 1996, **17**, 490.
17. Jorgensen, W. L. Maxwell, D. S. Tirado-Rives, J. *J. Am. Chem. Soc.* 1996, **118**, 11225.
18. MacKerell, A. D. Bashford, D. Bellott Dunbrack, R. L. Evanseck, J. D. Field, M. J. Fischer, S. Gao, J. Guo, H. Ha, S. Joseph-McCarthy, D. Kuchnir, L. Kuczera, K. Lau, F. T. K. Mattos, C. Michnick, S. Ngo, T. Nguyen, D. T. Prodhom, B. Reiher, W. E. Roux, B. Schlenkrich, M. Smith, J. C. State,

R. Straub, J. Watanabe, M. Wiórkiewicz-Kuczera, J. Yin, D. Karplus, M. *J. Phys. Chem. B* 1998, **102**, 3586.

19. Sun, H. *J. Phys. Chem. B* 1998, **102**, 7338.
20. Chen, B. Siepmann, J. I. *J. Phys. Chem. B* 1999, 103, 5370.
21. Cieplak, P. Caldwell, J. Kollman, P. *J. Comput. Chem.* 2001, **22**, 1048.
22. Kaminski, G. A. Friesner, R. A. Tirado-Rives, J. Jorgensen, W. L. *J. Phys. Chem. B* 2001, **105**, 6474.
23. Van Gunsteren, W. F. Daura, X. Mark, A. E. In *Encyclopedia of Computational Chemistry* John Wiley & Sons, Ltd, New York: 2002.
24. Duan, Y. Wu, C. Chowdhury, S. Lee, M. C. Xiong, G. Zhang, W. Yang, R. Cieplak, P. Luo, R. Lee, T. *J. Comput. Chem.* 2003, 24, 1999.
25. Wang, J. Wolf, R. M. Caldwell, J. W. Kollman, P. A. Case, D. A. *J. Comput. Chem.* 2004, **25**, 1157.
26. Oostenbrink, C. Villa, A. Mark, A. E. Van Gunsteren, W. F. *J. Comput. Chem.* 2004, **25**, 1656.
27. Brooks, B. R. Brooks, C. L. Mackerell, A. D. Nilsson, L. Petrella, R. J. Roux, B. Won, Y. Archontis, G. Bartels, C. Boresch, S. Caflisch, A. Caves, L. Cui, Q. Dinner, A. R. Feig, M. Fischer, S. Gao, J. Hodoscek, M. Im, W. Kuczera, K. Lazaridis, T. Ma, J. Ovchinnikov, V. Paci, E. Pastor, R. W. Post, C. B. Pu, J. Z. Schaefer, M. Tidor, B. Venable, R. M. Woodcock, H. L. Wu, X. Yang, W. York, D. M. Karplus, M. *J. Comput. Chem.* 2009, **30**, 1545.
28. Mackerell, A. D. *J. Comput. Chem.* 2004, **25**, 1584.
29. Dykstra, C. E. *J. Am. Chem. Soc.* 1989, **111**, 6168.
30. Bernardo, D. N. Ding, Y. Krogh-Jespersen, K. Levy, R. M. *J. Phys. Chem.* 1994, **98**, 4180.
31. Gao, J. Habibollazadeh, D. Shao, L. *J. Phys. Chem.* 1995, **99**, 16460.
32. Gao, J. Pavelites, J. J. Habibollazadeh, D. *J. Phys. Chem.* 1996, **100**, 2689.
33. Gao, J. *J. Comput. Chem.* 1997, **18**, 1061.
34. Dang, L. X. Chang, T.-M. *J. Chem. Phys.* 1997, **106**, 8149.
35. Chen, B. Xing, J. Siepmann, J. I. *J. Phys. Chem. B* 2000, **104**, 2391.
36. Saint-Martin, H. Hernández-Cobos, J. Bernal-Uruchurtu, M. I. Ortega-Blake, I. Berendsen, H. J. *J. Chem. Phys.* 2000, **113**, 10899.
37. Ren, P. Ponder, J. W. *J. Comput. Chem.* 2002, **23**, 1497.
38. Kaminski, G. A. Stern, H. A. Berne, B. J. Friesner, R. A. Cao, Y. X. Murphy, R. B. Zhou, R. Halgren, T. A. *J. Comput. Chem.* 2002, **23**, 1515.
39. Ren, P. Ponder, J. W. *J. Phys. Chem. B* 2003, **107**, 5933.
40. Kaminski, G. A. Stern, H. A. Berne, B. J. Friesner, R. A. *J. Phys. Chem. A* 2004, **108**, 621.

41. Patel, S. Mackerell, A. D. Brooks, C. L. *J. Comput. Chem.* 2004, **25**, 1504.
42. Yu, H. Van Gunsteren, W. F. *J. Chem. Phys.* 2004, **121**, 9549.
43. Wick, C. D. Stubbs, J. M. Rai, N. Siepmann, J. I. *J. Phys. Chem. B* 2005, **109**, 18974.
44. Lamoureux, G. Harder, E. Vorobyov, I. V. Roux, B. MacKerell, A. D. *Chem. Phys. Lett.* 2006, **418**, 245.
45. Gresh, N. Cisneros, G. A. Darden, T. A. Piquemal, J.-P. *J. Chem. Theory Comput.* 2007, **3**, 1960.
46. Xie, W. Pu, J. MacKerell, A. D. Gao, J. *J. Chem. Theory Comput.* 2007, **3**, 1878.
47. Lopes, P. E. Roux, B. MacKerell, A. D. *Theor. Chem. Acc.* 2009, **124**, 11.
48. Borodin, O. *J. Phys. Chem. B* 2009, **113**, 11463.
49. Xie, W. Pu, J. Gao, J. *J. Phys. Chem. A* 2009, **113**, 2109.
50. Shaw, D. E. Maragakis, P. Lindorff-Larsen, K. Piana, S. Dror, R. O. Eastwood, M. P. Bank, J. A. Jumper, J. M. Salmon, J. K. Shan, Y. Wriggers, W. *Science* 2010, **330**, 341.
51. Zhao, G. Perilla, J. R. Yufenyuy, E. L. Meng, X. Chen, B. Ning, J. Ahn, J. Gronenborn, A. M. Schulten, K. Aiken, C. Zhang, P. *Nature* 2013, **497**, 643.
52. Van Duin, A. C. Dasgupta, S. Lorant, F. Goddard, W. A. III. *J. Phys. Chem. A* 2001, **105**, 9396.
53. Brenner, D. W. Shenderova, O. A. Harrison, J. A. Stuart, S. J. NI, B. Sinnott, S. B. *J. Phys.: Condens. Matter* 2002, **14**, 783.
54. Nielson, K. D. van Duin, A. C. Oxgaard, J. Deng, W.-Q. Goddard, W. A. III *J. Phys. Chem. A* 2005, **109**, 493.
55. Zhao, M. Iron, M. A. Staszewski, P. Schultz, N. E. Valero, R. Truhlar, D. G. *J. Chem. Theory Comput.* 2009, **5**, 594.
56. Vesely, F. J. *J.Comput. Phys.* 1977, **24**, 361.
57. Howard, A. E. Singh, U. C. Billeter, M. Kollman, P. A. *J. Am. Chem. Soc.* 1988, **110**, 6984.
58. Pople, J. A. *Rev. Mod. Phys.* 1999, **71**, 1267.
59. Kohn, W. Becke, A. D. Parr, R. G. *J. Phys. Chem.* 1996, **100**, 12974.
60. Yang, W. *Phys. Rev. Lett.* 1991, **66**, 1438.
61. Gadre, S. R. Shirsat, R. N. Limaye, A. C. *J. Phys. Chem.* 1994, **98**, 9165.
62. Stewart, J. J. P. *Int. J. Quantum Chem.*, 1996, **58**, 133.
63. Dixon, S. L. Merz, K. M. *J. Chem. Phys.* 1996, **104**, 6643.
64. Dixon, S. L. Merz, K. M. *J. Chem. Phys.* 1997, **107**, 879.

65. Gao, J. *J. Phys. Chem. B* 1997, **101**, 657.
66. Gao, J. *J. Chem. Phys.* 1998, **109**, 2346.
67. Kitaura, K. Ikeo, E. Asada, T. Nakano, T. Uebayasi, M. *Chem. Phys. Lett.* 1999, **313**, 701.
68. Wierzchowski, S. J. Kofke, D. A. Gao, J. *J. Chem. Phys.* 2003, **119**, 7365.
69. Zhang, D. W. Zhang, J. Z. H. *J. Chem. Phys.* 2003, **119**, 3599.
70. Zhang, D. W. Xiang, Y. Zhang, J. Z. H. *J. Phys. Chem. B* 2003, **107**, 12039.
71. Hirata, S. Valiev, M. Dupuis, M. Xantheas, S. S. Sugiki, S. Sekino, H. *Mol. Phys.* 2005, **103**, 2255.
72. Collins, M. A. Deev, V. A. *J. Chem. Phys.* 2006, **125**
73. Dahlke, E. E. Truhlar, D. G. *J. Chem. Theory Comput.* 2006, **3**, 46.
74. Dahlke, E. E. Truhlar, D. G. *J. Chem. Theory Comput.* 2007, **3**, 1342.
75. Dułak, M. Kamiński, J. W. Wesołowski, T. A. *J. Chem. Theory Comput.* 2007, **3**, 735.
76. Li, W. Li, S. Jiang, Y. *J. Phys. Chem. A* 2007, **111**, 2193.
77. Xie, W. Gao, J. *J. Chem. Theory Comput.* 2007, **3**, 1890.
78. Hratchian, H. P. Parandekar, P. V. Raghavachari, K. Frisch, M. J. Vreven, T. *J. Chem. Phys.* 2008, **128**
79. Reinhardt, P. Piquemal, J.-P. Savin, A. *J. Chem. Theory Comput.* 2008, **4**, 2020.
80. Xie, W. Song, L. Truhlar, D. G. Gao, J. *J. Chem. Phys.* 2008, **128**
81. R?ezac?, J. Salahub, D. R. *J. Chem. Theory Comput.* 2009, **6**, 91.
82. Song, L. Han, J. Lin, Y.-I. Xie, W. Gao, J. *J. Phys. Chem. A* 2009, **113**, 11656.
83. Sode, O. Hirata, S. *J. Phys. Chem. A* 2010, **114**, 8873.
84. Gao, J. Cembran, A. Mo, Y. *J. Chem. Theory Comput.* 2010, **6**, 2402.
85. Gordon, M. S. Fedorov, D. G. Pruitt, S. R. Slipchenko, L. V. *Chem. Rev.* 2011, **112**, 632.
86. Jacobson, L. D. Herbert, J. M. *J. Chem. Phys.* 2011, **134**
87. Tempkin, J. O. B. Leverentz, H. R. Wang, B. Truhlar, D. G. *J. Phys. Chem. Lett.* 2011, **2**, 2141.
88. Mayhall, N. J. Raghavachari, K. *J. Chem. Theory Comput.* 2011, **7**, 1336.
89. Le, H.-A. Tan, H.-J. Ouyang, J. F. Bettens, R. P. *J. Chem. Theory Comput.* 2012, **8**, 469.
90. Wen, S. Nanda, K. Huang, Y. Beran, G. J. *Phys. Chem. Chem. Phys.* 2012, **14**, 7578.
91. Mayhall, N. J. Raghavachari, K. *J. Chem. Theory Comput.* 2012, **8**, 2669.

92. Wang, Y. Sosa, C. P. Cembran, A. Truhlar, D. G. Gao, J. *J. Phys. Chem. B* 2012, **116**, 6781.
93. Richard, R. M. Herbert, J. M. *J. Chem. Phys.* 2012, **137**, 064113.
94. Qi, H. W. Leverentz, H. R. Truhlar, D. G. *J. Phys. Chem. A* 2013, **117**, 4486.
95. Isegawa, M. Wang, B. Truhlar, D. G. *J. Chem. Theory Comput.* 2013, **9**, 1381.
96. Giese, T. J. York, D. M. *J. Chem. Phys.* 2007, **127**
97. Giese, T. J. Chen, H. Dissanayake, T. Giambaşu, G. M. Heldenbrand, H. Huang, M. Kuechler, E. R. Lee, T.-S. Panteva, M. T. Radak, B. K. York, D. M. *J. Chem. Theory Comput.* 2013, **9**, 1417.
98. Cembran, A. Bao, P. Wang, Y. Song, L. Truhlar, D. G. Gao, J. *J. Chem. Theory Comput.* 2010, **6**, 2469.
99. Gao, J. Wang, Y. *J. Chem. Phys.* 2012, **136**
100. Fedorov, D. G. Ishida, T. Kitaura, K. *J. Phys. Chem. A* 2005, **109**, 2638.
101. Hratchian, H. P. Krukau, A. V. Parandekar, P. V. Frisch, M. J. Raghavachari, K. *J. Chem. Phys.* 2011, **135**, 014105.
102. Xie, W. Orozco, M. Truhlar, D. G. Gao, J. *J. Chem. Theory Comput.* 2009, **5**, 459.
103. Löwdin, P. O. *J. Chem. Phys.* 1950, **18**, 365.
104. Mulliken, R. S. *J. Chem. Phys.* 1955, **23**, 1833.
105. Besler, B. H. Merz, K. M. Kollman, P. A. *J. Comput. Chem.* 1990, **11**, 431.
106. Wang, J. Cieplak, P. Kollman, P. A. *J. Comput. Chem.* 2000, **21**, 1049.
107. Leverentz, H. Gao, J. Truhlar, D. *Theor. Chem. Acc.* 2011, **129**, 3.
108. Momany, F. A. *J. Phys. Chem.* 1978, **82**, 592.
109. Cox, S. Williams, D. *J. Comput. Chem.* 1981, **2**, 304.
110. Singh, U. C. Kollman, P. A. *J. Comput. Chem.* 1984, **5**, 129.
111. Chirlian, L. E. Francl, M. M. *J. Comput. Chem.* 1987, **8**, 894.
112. Breneman, C. M. Wiberg, K. B. *J. Comput. Chem.* 1990, **11**, 361.
113. Wang, B. Truhlar, D. G. *J. Chem. Theory Comput.* 2012, **8**, 1989.
114. Storer, J. Giesen, D. Cramer, C. Truhlar, D. *J. Comput. Aided Mol. Des.* 1995, **9**, 87.
115. Marenich, A. V. Jerome, S. V. Cramer, C. J. Truhlar, D. G. *J. Chem. Theory Comput.* 2012, **8**, 527.
116. Zhang, P. Bao, P. Gao, J. *J. Comput. Chem.* 2011, **32**, 2127.
117. Frisch, M. J. Trucks, G. W. Schlegel, H. B. Scuseria, G. E. Robb, M. A. Cheeseman, J. R. Scalmani, G. Barone, V. Mennucci, B. Petersson, G. A.

Nakatsuji, H. Caricato, M. Li, X. Hratchian, H. P. Izmaylov, A. F. Bloino, J. Zheng, G. Sonnenberg, J. L. Hada, M. Ehara, M. Toyota, K. Fukuda, R. Hasegawa, J. Ishida, M. Nakajima, T. Honda, Y. Kitao, O. Nakai, H. Vreven, T. Montgomery, J. A., Jr. Peralta, J. E. Ogliaro, F. Bearpark, M. Heyd, J. J. Brothers, E. Kudin, K. N. Staroverov, V. N. Kobayashi, R. Normand, J. Raghavachari, K. Rendell, A. Burant, J. C. Iyengar, S. S. Tomasi, J. Cossi, M. Rega, N. Millam, N. J. Klene, M. Knox, J. E. Cross, J. B. Bakken, V. Adamo, C. Jaramillo, J. Gomperts, R. Stratmann, R. E. Yazyev, O. Austin, A. J. Cammi, R. Pomelli, C. Ochterski, J. W. Martin, R. L. Morokuma, K. Zakrzewski, V. G. Voth, G. A. Salvador, P. Dannenberg, J. J. Dapprich, S. Daniels, A. D. Farkas, Ö. Foresman, J. B. Ortiz, J. V. Cioslowski, J. Fox, D. J. *Gaussian Development Version* Gaussian Inc. Wallingford, CT, 2013

118. Zhao, Y. Truhlar, D. G. *Theor. Chem. Acc.* 2008, **120**, 215.
119. Lynch, B. J. Zhao, Y. Truhlar, D. G. *J. Phys. Chem. A* 2003, **107**, 1384.
120. Hehre, W. J. Ditchfield, R. Pople, J. A. *J. Chem. Phys.* 1972, **56**, 2257.
121. Phillips, J. C. Braun, R. Wang, W. Gumbart, J. Tajkhorshid, E. Villa, E. Chipot, C. Skeel, R. D. Kalé, L. Schulten, K. *J. Comput. Chem.* 2005, **26**, 1781.
122. Zhang, P. Fiedler, L. Leverentz, H. R. Truhlar, D. G. Gao, J. *J. Chem. Theory Comput.* 2011, **7**, 857.
123. Isegawa, M. Fiedler, L. Leverentz, H. R. Wang, Y. Nachimuthu, S. Gao, J. Truhlar, D. G. *J. Chem. Theory Comput.* 2012, **9**, 33.
124. Han, J. Mazack, M. J. M. Zhang, P. Truhlar, D. G. Gao, J. *J. Chem. Phys.* 2013, **139**, 054503.
125. Andersen, H. C. *J. Chem. Phys.* 1980, **72**, 2384.
126. Koopman, E. A. Lowe, C. P. *J. Chem. Phys.* 2006, **124**
127. Miyamoto, S. Kollman, P. A. *J. Comput. Chem.* 1992, **13**, 952.
128. Gao, J. Han, J. Zhang, P. *MCSOL version 2012xp* 2012
129. Mazack, M., J. M. Gao, J. *X-Pol. version 2013a1* 2013
130. Wang, B. Truhlar, D. G. *J. Chem. Theory Comput.* 2010, **6**, 3330.
131. Mo, Y. Gao, J. Peyerimhoff, S. D. *J. Chem. Phys.* 2000, **112**, 5530.
132. Mo, Y. Bao, P. Gao, J. *Phys. Chem. Chem. Phys.* 2011, **13**, 6760.
133. Pople, J. A. Santry, D. P. Segal, G. A. *J. Chem. Phys.* 1965, **43**, S129.
134. Cui, Q. Elstner, M. Kaxiras, E. Frauenheim, T. Karplus, M. *J. Phys. Chem. B* 2001, **105**, 569.
135. Elstner, M. *Theor. Chem. Acc.* 2006, **116**, 316.
136. Dewar, M. J. S. Thiel, W. *J. Am. Chem. Soc.* 1977, **99**, 4899.

137. Dewar, M. J. S. Thiel, W. *J. Am. Chem. Soc.* 1977, **99**, 4907.
138. Dewar, M. J. S. Thiel, W. *Theor. Chim. Acta* 1977, **46**, 89.
139. Fiedler, L. Gao, J. Truhlar, D. G. *J. Chem. Theory Comput.* 2011, **7**, 852.
140. Tang, K. T. Toennies, J. P. *J. Chem. Phys.* 1984, **80**, 3726.
141. Grimme, S. Antony, J. Ehrlich, S. Krieg, H. *J. Chem. Phys.* 2010, **132**
142. Grimme, S. Ehrlich, S. Goerigk, L. *J. Comput. Chem.* 2011, **32**, 1456.
143. McNamara, J. P. Hillier, I. H. *Phys. Chem. Chem. Phys.* 2007, **9**, 2362.
144. Morgado, C. A. McNamara, J. P. Hillier, I. H. Burton, N. A. Vincent, M. A. *J. Chem. Theory Comput.* 2007, **3**, 1656.
145. McNamara, J. P. Sharma, R. Vincent, M. A. Hillier, I. H. Morgado, C. A. *Phys. Chem. Chem. Phys.* 2008, **10**, 128.
146. Chang, D. T. Schenter, G. K. Garrett, B. C. *J. Chem. Phys.* 2008, **128**, 164111.
147. Habershon, S. Markland, T. E. Manolopoulos, D. E. *J. Chem. Phys.* 2009, **131**, 024501.
148. Stern, H. A. Berne, B. *J. Chem. Phys.* 2001, **115**, 7622.
149. Murdachaew, G. Mundy, C. J. Schenter, G. K. Laino, T. Hutter, J. *J. Phys. Chem. A* 2011, **115**, 6046.
150. Stewart, J. J. P. *J. Comput. Chem.* 1989, **10**, 209.
151. Stewart, J. J. P. *J. Mol. Model.* 2007, **13**, 1173.
152. Silvestrelli, P. L. Parrinello, M. *Phys. Rev. Lett.* 1999, **82**, 3308.
153. Coulson, C. A. Eisenberg, D. *Proc. R. Soc. London Ser. A* 1966, **291**, 445.
154. Caldwell, J. W. Kollman, P. A. *J. Phys. Chem.* 1995, **99**, 6208.
155. Sprik, M. *J. Chem. Phys.* 1991, **95**, 6762.
156. Lamoureux, G. MacKerell, A. D. Roux, B. *J. Chem. Phys.* 2003, **119**, 5185.
157. Soper, A. *Chem. Phys.* 2000, **258**, 121.
158. Head-Gordon, T., Johnson, M. E. *Proc. Natl. Acad. Sci.* 2006, **103**, 7973.

approach the explicit polarization (X-Pol) method. Strategies and examples are presented to illustrate the application of X-Pol to describe intermolecular interactions as a quantum chemical model and as a force field to carry out statistical mechanical Monte Carlo and molecular dynamics simulations.

2.1 Introduction

Molecular mechanical force fields (MMFFs) were first proposed in the 1940s to study steric effects of organic molecules[1,2] and were extended to model biomolecular systems by Lifson and coworkers in the 1960s.[3–5] Since that time, significant progress has been made, and a number of force fields have been developed that can be used to provide excellent quantitative interpretation of experimental observations.[6–27]

Although the widely used force fields differ in their details (for example, some of them include coupling between internal coordinates), the functional forms used in MMFFs have remained essentially unchanged over the past half century,[5,28] and the functional form depicted in Eq. 2.1 captures the essence of a typical MMFF potential energy function:

$$V = \sum_{b}^{\text{bonds}} \frac{1}{2} K_b (R_b - R_b^o)^2 + \sum_{a}^{\text{angles}} \frac{1}{2} K_a (\theta_a - \theta_a^o)^2 + \sum_{t}^{\text{torsion}} \sum_{n} \frac{V_t^n}{2} [1 + \cos(n\phi_t - \phi_t^o)] + \sum_{i<j} \left\{ \varepsilon_{ij} \left[\left(\frac{\sigma_{ij}}{R_{ij}} \right)^{12} - \left(\frac{\sigma_{ij}}{R_{ij}} \right)^{6} \right] + \frac{q_i q_j}{R_{ij}} \right\} \quad (2.1)$$

In this equation, the first sum accounts for bond stretching, the second sum for valence angle bending, the third (double) sum for torsions, and the fourth, where the sum goes only over nonbonded and nongeminal atoms, for van der Waals interactions and nonbonded Coulomb forces.

The importance of polarization has long been recognized, and Eq. (2.1) includes polarization implicitly through the choice of

parameters, which are often designed to include not just the effect of intramolecular polarization but also the effect of polarization by the solvent or other surroundings in a condensed-phase medium. Major current efforts in improving MMFFs are being devoted to the explicit inclusion of polarization by means of terms of various forms to account for inductive forces.[29–49] We will label force fields that include polarization explicitly as polarized molecular mechanics force fields or PMMFFs, while we restrict the acronym MMFFs to force fields that include polarization only implicitly through the parametrization.

Despite the success of molecular mechanics,[28,50,51] there are also a number of limitations: There is no general approach to treat the coupling of internal degrees freedom, the treatment of electronic polarization is difficult, intermolecular charge transfer is neglected, excited electronic states cannot be treated, and in the form usually employed the methods are inapplicable to chemical reactions.[28] In recent years, some extensions to treat chemically reactive systems have been presented,[52–55] and one can overcome some of the limitations in specific applications by introducing additional empirical terms,[31,32,56,57] but here we discuss another approach, where the whole treatment is intrinsically based on quantum mechanics (QM).

Quantum mechanical electronic structure calculations can provide both reactive and nonreactive potential energy surfaces, including not only electrostatics and van der Waals forces but also polarization and charge transfer effects. However, it is a daunting task (essentially impossible) to solve the Schrödinger equation for a condensed-phase system. Therefore, a wide range of approximate quantum chemical model chemistries have been developed, including both wave function theory (WFT)[58] and density functional theory (DFT),[59] as well as various linear scaling and fragment-based QM methods that have been proposed to reduce the computation costs.[60–95] The latter represents an active approach to balance accuracy and efficiency in applying electronic structural methods to large systems.

The explicit polarization (X-Pol) model is a fragment-based QM method, in which the entire system is divided into molecular subunits,[65,66,77,80] which can be individual molecules, ions, ligands

or cofactors, and amino acid residues or a group of these entities. The key assumption in the X-Pol method is that the wave function of the entire system is approximated as a Hartree product of the wave functions of the individual fragments. Consequently, the optimization of the total wave function can be reduced to the optimization of each fragment embedded in and polarized by the rest of the system. Clearly, variational optimization of the mutual dependence of the fragmental wave functions is critical to the success of this method. As a force field, the energy of each fragment corresponding to the intramolecular energy terms in an MMFF is determined by the electronic structure method used, whereas intermolecular interactions are modeled through electrostatic embedding in terms of one-electron integrals. The short-range exchange repulsion interactions between fragments, the long-range dispersion interactions between different fragments, and the interfragment correlation energy are neglected in the Hartree product approximation but are modeled empirically as in molecular mechanics.[65,66,77] Alternatively, these energy contributions can be modeled by density-dependent functional,[96,97] by Hartree–Fock (HF) exchange,[98] or by making use of many-body expansion corrections.[99] The latter also takes into account interfragment charge transfer effects, which are otherwise neglected, although intrafragment charge transfer is fully included. X-Pol[92] can also be used as a general QM-QM fragment-coupling scheme,[88,100,101] in which different levels of theory are employed to model different fragments; we refer to this as a multilevel method.

In the following sections, we summarize the theoretical formulation of the X-Pol model and illustrate the multilevel X-Pol[92] method for studying intermolecular interactions. In addition, we discuss our work on using X-Pol as a quantum mechanical force field (QMFF) for liquid water simulations.

2.2 Theoretical Background

In X-Pol, a macromolecular system is partitioned into molecular fragments, which may be called monomers. The division is flexible within the constraint that monomers do not overlap, (i.e., the

subsystem included in one fragment does not appear in another monomer). For solutions with small solute molecules, a fragment can be a single solute or solvent molecule.[65,66] For large solute molecules or biomacromolecules, (e.g., a protein or enzyme–substrate complex) a fragment can be a connected group of atoms (e.g., peptide unit, or a metal atom or ion, a cofactor, or a substrate molecule).[77,102] Several peptide units can be combined into the same fragment, if desired, which can be useful for modeling systems containing disulfide bonds. The X-Pol method is derived from a standard electronic structure method by a nested set of three approximations, described next.

2.2.1 *Approximation of the Total Wave Function and Total Energy*

The first approximation in the X-Pol theory is that the molecular wave function of the entire system Ψ is approximated as a Hartree product of the antisymmetric wave functions of individual fragments, $\{\Psi_A; A = 1, \cdots, N\}$:

$$\Psi = \prod_{A=1}^{N} \Psi_A. \tag{2.2}$$

The wave function of fragment A, Ψ_A, can either be a single determinant from HF theory or Kohn–Sham DFT, or a multiconfiguration wave function derived from complete active space self-consistent field (CASSCF) or valence bond (VB) calculations.

The effective Hamiltonian of the system is expressed as Eq. 2.3

$$\hat{H} = \sum_{A}^{N} \hat{H}_A^o + \frac{1}{2}\sum_{A}^{N}\sum_{B\neq A}^{N}(\hat{H}_A^{int}[\rho_B] + E_{AB}^{XD}), \tag{2.3}$$

where the first term sums over the Hamiltonians of all isolated fragments and the second double summation accounts for pairwise interactions among all the fragments. The explicit form of $\hat{H}_A^o$, which is the Hamiltonian for an isolated fragment A in the gas phase, varies according to the level of theory employed, for instance, post-HF correlated methods can be used to treat the active site of an enzyme, and HF or semiempirical molecular orbital methods can be used to treat solvent molecules or peptide units that are distant from the

reactive center. The Hamiltonian $\hat{H}_A^{int}[\rho_B]$ represents electrostatic interactions between fragments A and B, and the final term E_{AB}^{XD} specifies exchange-repulsion, dispersion and other interfragment correlation energy contributions, and charge transfer interactions, as explained in more detail in the following sections.

The total energy of the system is written as the expectation value of the effective Hamiltonian,

$$E[\{\rho\}] = <\Psi|H|\Psi> \; = \sum_A^N E_A + \frac{1}{2}\sum_A^N \sum_{B\neq A}^N (E_{AB}^{int}[\rho_A, \rho_B] + E_{AB}^{XD}) \tag{2.4}$$

where E_A is the energy of fragment A that is determined using its wave function as *polarized* by all other fragments, and $E_{AB}^{int}[\rho_A, \rho_B]$ is the electrostatic interaction energy between fragments A and B, again calculated using the polarized wave functions. The latter term is calculated from the point of view of fragment A and also from the point of view of fragment B, and the sum of these results is divided by two since the same interactions are counted twice. Therefore, we have

$$E_A = <\Psi_A|\hat{H}_A^0|\Psi_A>, \tag{2.5}$$

$$E_{AB}^{int}[\rho_A, \rho_B] = \frac{1}{2}\left(<\Psi_A|\hat{H}_A^{int}[\rho_B]|\Psi_A> + <\Psi_B|\hat{H}_B^{int}[\rho_A]|\Psi_B>\right). \tag{2.6}$$

2.2.2 *Approximation on the Electrostatic Interaction between Fragments*

The second approximation in the X-Pol theory is the method of treating the interaction between fragments. The interaction Hamiltonian between fragment A and B is defined as

$$\hat{H}_A^{int}[\rho_B] = -\sum_{i=1}^{M_A} e\,\Phi_E^B(\mathbf{r}_i^A) + \sum_{\alpha=1}^{N_A} Z_\alpha^A \Phi_E^B(\mathbf{R}_\alpha^A), \tag{2.7}$$

where M_A and N_A are respectively the number of electrons and nuclei in fragment A, Z_α^A is the nuclear charge of atom α of fragment A, and $\Phi_E^B(\mathbf{r}_x^A)$ is the electrostatic potential at $\mathbf{r}_x$ from fragment B. The electrostatic potential is given by

$$\Phi_E^B(\mathbf{r}_x^A) = \int \frac{\rho_B(\mathbf{r}')}{|\mathbf{r}_x^A - \mathbf{r}'|} d\mathbf{r}', \tag{2.8}$$

where $\rho_B(\mathbf{r}') = -\rho_{ele}^B(\mathbf{r}') + \sum_\beta Z_\beta^B \delta(\mathbf{r}' - \mathbf{R}_\beta^B)$ is the total charge density of fragment B, including electron density $\rho_{ele}^B(\mathbf{r}')$ and nuclear charge Z_β^B at $\mathbf{R}_\beta^B$. The potential $\Phi_E^B(\mathbf{r}_x^A)$ can be used directly to determine the electrostatic interaction energy of Eq. 2.7; this involves or is equivalent to evaluating the corresponding four-index two-electron integrals explicitly, which is time-consuming and could be ill-behaved when large basis sets are used. Although it yields the classical electrostatic part of the interaction without approximation, it does not include the exchange repulsion part of the interfragment interaction or the interfragment correlation energy, which will be discussed in Section 2.2.3. To reduce the computational cost in two-electron integral calculation, it is desirable to an efficient approach to treat interfragment electrostatic interactions.[65,66]

The quantity $\Phi_E^B(\mathbf{r}_x^A)$ may be considered as an embedding potential of fragment A due to the external charge distribution of fragment B, and a number of well-established techniques.[15,21,103–107] can be used to model it. A general approach for the classical electrostatic potential is to use a multicenter multipole expansion,[107] of which the simplest form is to limit the expansion to the monopole terms, so the result only depends on the partial atomic charges. The use of partial atomic charges to approximate $\Phi_E^B(\mathbf{r}_x^A)$ is particularly convenient for constructing the effective Hamiltonian of Eq. 2.7, and this is the strategy that has been adopted for the classical electrostatic part in the X-Pol method.[65,66]

The next issue in modeling the electrostatic interaction is the method to obtain the monopole charges. For these charges, one may use partial atomic charges fitted to the electrostatic potential (ESP)[15,105,106 108–113] or one may use Mulliken population analysis,[104] population analysis based on Löwdin orthogonalization,[103] or class IV charges from mapping procedures[114,115] in which the mapping function has been parametrized to yield atomic charges that reproduce experimental molecular dipole moments. Another method is based on optimization of atomic charges to reproduce the molecular multipole moments from QM calculations, and we have recently used a procedure that preserves the molecular dipole moment and polarizability to generate dipole-preserving and polarization-consistent charges (DPPCs).[116]

Using the approximation of point charges, Eq. 2.8 is simplified to

$$\Phi_{\mathrm{E}}^{B}(\mathbf{r}_x^A) = \sum_{\beta} \frac{q_\beta^B}{|\mathbf{r}_x^A - \mathbf{R}_\beta^B|}. \tag{2.9}$$

2.2.3 *Approximations to Interfragment Exchange–Dispersion Interactions*

The Hartree product wave function in Eq. 2.2 neglects the long-range interfragment dispersion interactions, the other interfragment correlation energy contributions, and the short-range interfragment exchange-repulsion interactions arising from the Pauli exclusion principle. Furthermore, the partition of a molecular system into fragments and the restriction to an integer number of electrons in each fragment precludes charge transfer between the fragments. But interfragment dispersion interactions, the other interfragment correlation energy contributions, the short-range exchange-repulsion interactions, and charge transfer make critical contributions to intermolecular interactions, so they must be added to the X-Pol energy expression. A brute force approach is to employ variational many-body expansion (VMB) theory to make two-body, three-body, and higher order corrections.[99] Although the accuracy can be systematically improved by using many-body corrections, the number of terms involved increases rapidly with the number of fragments and the order of correction, rendering this approach impractical beyond two-body correction terms. Thus in using this approach, it is critical to define the reference state for the monomer energies such that the higher-order correction terms are negligible. However, when the X-Pol method is used as a theoretical framework to develop force fields for condensed-phase and macromolecular systems, we can use a simpler approach. In particular, we introduce empirical terms such as Lennard-Jones or Buckingham potentials (as used in molecular mechanics) to estimate the exchange repulsion, dispersion, other interfragment correlation, and charge transfer energies. In one of the applications described in Section 2.4.1,[92] we add the following pairwise Buckingham-potential term to the interaction energy between fragments A and B:

$$E_{AB}^{\mathrm{XD}} = \sum_{I}^{N_A} \sum_{J}^{N_B} \left(A_{IJ} e^{-B_{IJ} \cdot R_{IJ}} - \frac{C_{IJ}}{R_{IJ}^6} \right) \tag{2.10}$$

where the parameters are determined from the atomic parameters according to combining rules:

$$A_{IJ} = (A_I A_J)^{1/2} \tag{2.11}$$

$$B_{IJ} = (B_I + B_J)/2 \tag{2.12}$$

$$C_{IJ} = (C_I C_J)^{1/2} \tag{2.13}$$

In the other application discussed in Section 2.4.2, we used pairwise Lennard-Jones potentials.

2.2.4 *Double Self-Consistent Field*

As in standard electronic structure methods, the Roothaan–Hall equation on each fragment in X-Pol is solved iteratively. However, in X-Pol, in addition to the SCF convergence within each molecular fragment, the mutual polarization among all fragments of the whole system must be converged. A procedure is depicted in Fig. 2.1, which may be described as a double self-consistent field (DSCF) iterative scheme. In practice, however, there is no need to fully converge the inner, intrafragment SCF before proceeding to the next iteration step for the outer, interfragment SCF. We found that it is often computationally efficient to carry out two to three iterations in the intrafragment SCF between the outer SCF iterations.

There are two ways of constructing the Fock matrix for solving the DSCF equations; one is based on the variational optimization of the energy of Eq. 2.4,[80] and the other, which was first used in Monte Carlo simulations where analytic forces are not required,[65,66] is written by assuming that each monomer is embedded in the fixed electrostatic field of the rest of the system. The two approaches are discussed next.

(a) Variational X-Pol. In X-Pol, the Fock operator for a fragment, A, is derived by taking the derivative of the total energy (Eq. 2.4) with

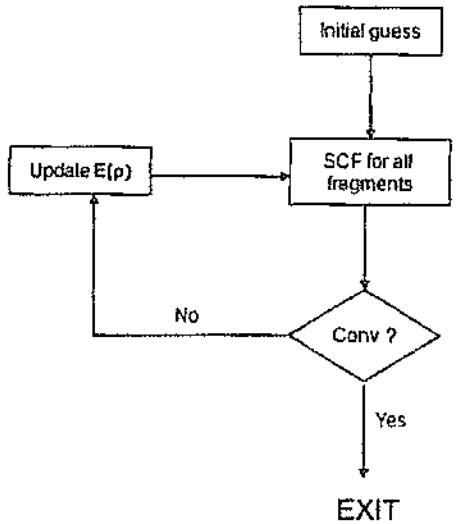

Figure 2.1 The schematic flow chart of DSCF iterations.

respect to each element $P^A_{\mu\nu}$ of the electron density matrix:

$$\mathbf{F}^{A,\mathrm{Xpol}}_{\mu\nu} = \frac{\partial E[\{\rho\}]}{\partial P^{A,SCF}_{\mu\nu}} = \mathbf{F}^{A,o}_{\mu\nu} - \frac{1}{2}\sum_{B\neq A}\sum_{b\in B} q^B_b \left(\mathbf{I}^B_b\right)^A_{\mu\nu} - \frac{1}{2}\sum_{a\in A} X^A_a \left(\Lambda^A_a\right)_{\mu\nu}, \tag{2.14}$$

where $\mathbf{F}^{A,o}_{\mu\nu}$ is the Fock matrix element for the Hamiltonian of the isolated fragment A, q^B_b is the point charge on atom b of fragment B, $\mathbf{I}^B_b$ is the matrix of the one-electron integrals of the embedding potential due to fragment B, X^A_a is a vector arising from the derivative of the electrostatic interaction energy with respect to the point charge of atom a:

$$X^A_a = \sum_{B\neq A}\left(\sum_{\lambda\sigma} P^B_{\lambda\sigma}\left(\mathbf{I}^A_a\right)^B_{\lambda\sigma} + \sum_{b\in B}\frac{Z^B_b}{|\mathbf{R}^B_b - \mathbf{R}^A_a|}\right), \tag{2.15}$$

and Λ^A_a is the response density matrix:

$$\left(\Lambda^A_a\right)_{\mu\nu} = \frac{\partial q^A_a}{\partial P^{A,\mathrm{SCF}}_{\mu\nu}} = \frac{\partial q^{A,\mathrm{SCF}}_a}{\partial P^{A,\mathrm{SCF}}_{\mu\nu}}. \tag{2.16}$$

(b) Charge-embedding X-Pol. If each fragment is considered to be embedded in the instantaneous static electrostatic field of the rest of the system, one can construct a Fock operator for fragment A simply as follows:

$$\mathbf{F}^{A,CE} = \mathbf{F}^{A,o} - \sum_{B\neq A}\sum_{b\in B} q^B_b \left(\mathbf{I}^B_b\right)^A. \tag{2.17}$$

In the charge-embedding approach, the mutual polarization among all fragments in the system is achieved by iteratively updating the partial atomic charges $\{q^B_b\}$ derived from the wave function for each fragment in each outer, interfragment SCF step (Fig. 2.1). Note that Eq. 2.14 indicates that the wave function of each fragment, A, is fully polarized by the full electric field of all other fragments, but the total interaction energy will be determined by multiplying a factor of 0.5 since the interactions between two monomers are counted twice. Similar expressions are often found in continuum self-consistent reaction field models for solvation.

Comparison. In comparing methods a and b, we note that the variational X-Pol method has the advantage of allowing the computation of analytic gradients for efficient geometry optimization and dynamics simulations. Furthermore, the total energy obtained from the variational procedure is necessarily lower than that from the charge-embedding scheme. Consequently, it is expected that the use of the variational X-Pol energy as the monomer energy reference state in many-body energy expansion be more efficient than other alternatives. Although it is possible to obtain analytic gradients for the non-variational, charge-embedding approaches, it generally involves solution of coupled-perturbed self-consistent field (CPSCF) equations, which is more time consuming. As a referee of this manuscript lucidly pointed out, "often in the fragment quantum chemistry literature, those response terms have simply been ignored, with numerical consequences that have never been investigated."

2.3 Computational Details

The X-Pol method has been implemented in a developmental version of the Gaussian software package (H35).[117] Although a single quantum chemical model can be used to represent all fragments, any of the electronic structure methods available in Gaussian, such as HF, DFT, MP2, CCSD, BD, etc., can be mixed to represent different fragments in a multilevel X-Pol calculation. We have illustrated the multilevel approach in a recent study[92] of two hydrogen-bonded complexes, including (a) acetic acid (fragment A) and water (fragment B), and (b) $H_5O_2^+$ ion (fragment A) and four surrounding water molecules (fragments B, five fragments in total). In that work, the geometries of the complexes and isolated monomers were optimized using the M06 exchange-correlation functional[118] and the MG3S[119] basis set, which was followed by single-point, multilevel X-Pol calculations using the 6-31G(d)[120] basis set.

For condensed-phase and macromolecular simulations, we have written an X-Pol software package using the C++ language, which has been incorporated into NAMD[121] and CHARMM.[27] The X-Pol program can be used with the popular NDDO-based semiempirical Hamiltonians as well as the recently developed polarized molecular orbital (PMO) model.[122,123] Molecular dynamics simulations of liquid water have been carried out using the NAMD/X-Pol interface. In addition, we have used an earlier version of the X-Pol model in Monte Carlo simulations of liquid water.

Statistical mechanical Monte Carlo simulations were performed on a system consisting of 267 water molecules in a cubic box, employing the XP3P water model, built upon the PMOw Hamiltonian[124] and the DPPC charge model.[116] Periodic boundary conditions were used along with the isothermal-isobaric ensemble (NPT) at 1 atm and for a temperature ranging from −40 to 100 C. Spherical cutoffs with a switching function between 8.5 Å and 9.0 Å based on oxygen–oxygen separations were employed, and a long-range correction to the Lennard–Jones potential was included. In Monte Carlo simulations, new configurations were generated by randomly translating and rotating a randomly selected water molecule within ranges of ± 0.13 Å and ± 13 . In addition, the volume of the system was changed randomly within the limit of ± 150 Å^3 on every 550th attempted move, and the coordinates of oxygen atoms were scaled accordingly. At least 5×10^6 configurations were discarded for equilibration, followed by an additional 10^7 to 10^8 configurations for averaging. About 6×10^6 configurations can be executed per day on a six-core Intel Xeon X7542 Westmere 2.66 GHz processor.

The XP3P model was further employed in molecular dynamics simulations for 500 ps in the NVT ensemble using the Lowe-Andersen thermostat.[125,126] The volume was fixed at the average value from the Monte Carlo simulation. The monomer geometries were enforced by the SHAKE/RATTLE procedure.[127] The velocity Verlet integration algorithm was used with a 1fs time step. The Monte Carlo simulations were performed using the MCSOL program for X-Pol simulations,[128] while molecular dynamics simulations were carried out using a newly developed X-Pol program[129] written in C++ which has been interfaced both with CHARMM[27] and NAMD.[121]

2.4 Illustrative Examples

2.4.1 *Multilevel X-Pol as a Quantum Chemical Model for Macromolecules*

The X-Pol theory can be used with a combination of different electronic structure methods for different fragments. This provides a general, multi-level QM/QM-type of treatment of a large system, where the region of interest could be modeled by a high-level theory, embedded in an environment modeled by a lower level representation. Some arbitrary combinations of different electronic models are illustrated by calculations[92] of the interaction energy between acetic acid and water at the minimum-energy configuration optimized with M06/MG3S (Fig. 2.2). To represent the electrostatic potential in Eq. 2.9, we used two charge models, Mulliken population analysis (MPA) and ESP charge-fitting with the Merz–Kollman scheme (MK), to construct the charge-embedding Fock matrix (Eq. 2.14), whereas only the MPA charges were used in variational X-Pol (Eq. 2.11).

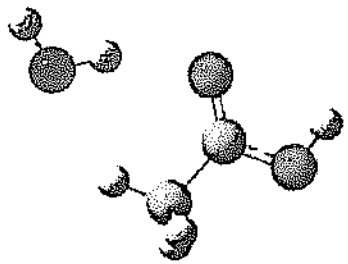

Figure 2.2 Schematic illustration of the optimized configuration of acetic acid and water using M06/MG3S.

The binding energy for a bimolecular complex is defined by

$$\Delta E_b = E_{AB} - E_A^o - E_B^o \tag{2.18}$$

(We have not applied any correction for the basis set superposition error since the main purpose here is to illustrate the possibility of mixing different levels of theory in multi-level X-Pol calculations.) In X-Pol, the binding energy is written as the sum of electrostatic (ΔE_{elec}) and exchange-charge transfer-dispersion (ΔE_{XCD}) terms.

$$\Delta E_b = \Delta E_{\text{elec}} + \Delta E_{\text{XCD}}, \tag{2.19}$$

where the electrostatic interaction energy in X-Pol is given by

$$\Delta E_{\text{elec}} = \frac{1}{2}[E_A^{int}(B) + E_B^{int}(A)] + (E_A - E_A^o) + (E_B - E_B^o), \tag{2.20}$$

where $E_X^{int}(Y)$ represents the interaction of "QM" fragment X polarized by the electrostatic potential from fragment Y, and $(E_X - E_X^o)$ is the energy difference between fragment X in the complex and in isolation. Table 2.1 summarizes the results from these calculations.

The ΔE_{XCD} term can be determined by VMB expansion. For the bimolecular complex in Fig. 2.2, the two-body correction energy is exact. For condensed-phase and macromolecular systems, it is convenient to simply approximate ΔE_{XCD} by an empirical potential such as the Lennard–Jones potential or the Buckingham potential.

The total binding energy between acetic acid and water were estimated to be −6.9 and −6.6 kcal/mol from M06/MG3S and CCSD(T)/MG3S, respectively. Therefore, Table 2.1 shows that the

Table 2.1 Computed electrostatic interactions energies ΔE_{elec} (kcal/mol) between acetic acid (A) and water (B) using multilevel X-Pol with the charge-embedding and variational interaction Hamiltonians

A	B	Charge-embedding		Variational	Full QM[a]
		MK-ESP	MPA	MPA	
M06	M06	−7.0	−7.7	−9.0	−6.9
M06	B3LYP	−6.8	7.3	−8.7	−6.9
M06	HF	−7.2	7.9	9.4	−6.9
MP2	HF	−7.1	−7.7	−8.0	−6.5
CCSD	M06	−7.2	7.6	−8.0	−6.6[b]

Note: The 6-31G(d) basis set was used in all calculations with the M06/MG3S optimized monomer and dimer geometries.
[a]Computed for the complex using the method listed under A with the MG3S basis set.
[b]Determined using CCSD(T)

approximate electrostatic components computed by the X-Pol method overestimate binding interactions for all combinations of methods examined except the combination of M06 for acetic acid and B3LYP for water. Within the charge-embedding scheme, the use of ESP-fitted charges resulted in somewhat weaker binding interactions than those from Mulliken population analysis. However, the variational approach yielded binging energies about 1–2 kcal/mol greater than the corresponding embedding model; at the M06/6-31G(d) level, the binding energy difference between the variational X-Pol result and reference value is about 2 kcal/mol. An empirical correction based on the Buckingham potential, dominated by the first term that represent exchange repulsion, gives a correction of 2.1 kcal/mol, and if this is added to the electrostatic terms, the total X-Pol results obtained using the variational approach become more consistent with the values from fully delocalized calculations.

Table 2.2 shows the computed electrostatic interaction energies and the empirical ΔE_{XCD} correction term for a protonated water cluster using the multilevel X-Pol scheme. The protonated water cluster is a Zundel ion $H_5O_2^+$ with four water molecules; the optimized structure of the complex obtained by the M06/MG3S method is illustrated in Fig. 2.3. Next we analyze the individual

Table 2.2 Computed electrostatic interactions energies ΔE_{elec} (kcal/mol) between $H_5O_2^+$ (A) and $(H_2O)_4$ (B) using multilevel X-Pol with the charge-embedding and variational interaction Hamiltonians

A	B	Charge-embedding		Variational		
		MK-ESP	MPA	MPA	ΔE_{XCD}	ΔE_b
M06	M06	−89.1	−87.5	−91.0	18.2	−72.8
M06	B3LYP	−87.7	−85.2	−88.1	18.2	−69.9
M06	HF	−92.0	−91.7	−94.5	18.2	−76.3
MP2	HF	−92.9	−92.7	−94.4	18.2	−76.2
CCSD	M06	−89.5	−88.0	−83.9	18.2	−65.7

Note: The 6-31G(d) basis set was used in all calculations with M06/MG3S optimized monomer and dimer geometries.

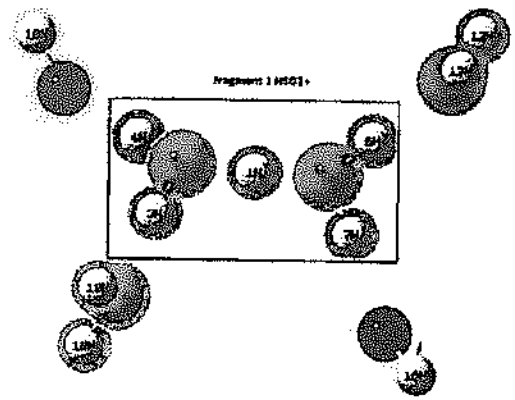

Figure 2.3 Fragment partition of the $H_5O_2^+(H_2O)_4$ cluster optimized using M06/MG3S.

contributions from exchange-repulsion, dispersion and charge transfer interactions.

As explained elsewhere,[98] exchange repulsion can be obtained as the difference between the energy from the antisymmetrized X-Pol wave function for the two fragments, $\hat{A}\{\Psi_A\Psi_B\}$, and the X-Pol electrostatic interaction energy ΔE_{ele} obtained at the SCF level. Using M06/6-31G(d), the charge-embedding scheme yielded an

exchange repulsion energy of 30.0 kcal/mol with the MK charge model and 28.5 kcal/mol with the MPA charge scheme. This may be compared with a value of 35.8 kcal/mol from variational X-Pol using MPA. The difference between the non-variational charge-embedding scheme and the variational X-Pol result shows that there is charge penetration between the two monomer fragments, but the use of unscreened point-charge interactions does not account for this.[130] Note that the exchange energy described above was estimated using the X-Pol electrostatic energy, which is an approximation to the two-electron repulsion integrals between the two fragments, as explained in Section 2.2.2.

The exchange repulsion energy can be obtained more rigorously by block localized energy decomposition analysis,[131,132] and we have carried out this analysis for the complex at the HF/aug-cc-pVDZ level. The computed exchange-repulsion and charge transfer energies are 38.8 kcal/mol and −13.3 kcal/mol, with a net contribution of 25.5 kcal/mol from the two energy terms.

The dispersion-correlation energy can be defined as the difference between the interaction energy computed using an accurate post-Hartree–Fock method and that at the Hartree–Fock level, both corrected by basis set superposition errors. Here, we have not included the BSSE correction contributions, which will affect the quantitative results. Based on the binding energies calculated by CCSD(T)/MG3S (−69.7 kcal/mol) and by HF/aug-cc-pVDZ (−62.4 kcal/mol), we estimate a dispersion-correlation energy of −7.3 kcal/mol. The sum of these terms, that is, 25.5 minus 7.3 kcal/mol, which includes exchange repulsion, charge transfer, and dispersion-correlation, gives an estimate of the ΔE_{XCD} term, which is 18.2 kcal/mol for the interactions between the Zundel ion and four water molecules. Including the ΔE_{XCD} energy, we find that the total X-Pol binding energies from various multilevel calculation range from −65 to −76 kcal/mol, which may be compared with the binding energy computed using CCSD(T)/MG3S (−69.7 kcal/mol) for the full system. The discrepancy between the X-Pol results and full QM results has several contributing factors, chief of which include fixed geometry at a different level of theory and basis set, and the use of a rather small basis set in the X-Pol calculations. Without including ΔE_{XCD}, the binding energies for different X-Pol calculations range

from −83 and −92 kcal/mol, all significantly greater than the full QM value.

2.4.2 *The XP3P Model for Water as a Quantum Mechanical Force Field*

Although ab initio molecular orbital theory and density functional theory can be used to systematically improve the accuracy of X-Pol results for large systems, it is still impractical to use these methods to perform molecular dynamics simulations for an extended period of time. With increased computing power, this will become feasible in the future; however, at present, it is desirable to use semiempirical molecular orbital models such as the popular approaches based on neglect of diatomic differential overlap (NDDO)[133] or the more recent self-consistent-charge tight-binding density functional (SCC-DFTB)[134,135] method to model condensed-phase and biomacromolecules.

Most semiempirical molecular orbital methods are known to be inadequate to describe intermolecular interactions, especially on hydrogen bonding interactions because molecular polarizabilities are systematically underestimated in comparison with experiments. Recently, we introduced a polarized molecular orbital (PMO) method[122–123] which is based on the MNDO[136–138] formalism with the addition of a set of *p*-orbitals on each hydrogen atom.[139] It was found that the computed molecular polarizabilities for a range of compounds containing hydrogen, carbon and oxygen are very significantly improved.[122,123] In addition to the enhancement in computed molecular polarizability, a damped dispersion function is included as a post-SCF correction to the electronic energy. In principle, the Lennard–Jones terms originally adopted in the X-Pol method could be used.[66] Here, we added damped dispersion by following the work of, among others, Tang and Toennies in wave function theory[140] and Grimme in density functional theory[141,142] and we used the parameters proposed by Hillier and co-workers in the PM3-D method.[143–145] The inclusion of the damped dispersion terms further improves the description of intermolecular interactions and the performance of PMO on small molecular clusters.

We note one previous model similar in spirit to PMO, namely the semiempirical self-consistent polarization neglect of diatomic differential overlap (SCP-NDDO) method, parametrized to reproduce properties of water clusters by Chang et al.[146] They obtained a good polarizability of water without using *p* functions on hydrogen (i.e., they used the minimal basis set employed in most NDDO calculations), but their model is parametrized only for water. Since a minimal basis set does not have the flexibility to yield an accurate polarizability in ab initio calculations,[139] it is not clear if the SCP-NDDO-type parametrization could be extended to a broader range of molecules.

The construction of a QMFF based on the X-Pol formalism has two components. First, a computationally efficient quantum chemical model is needed to describe the electronic structure of individual molecular fragments. For liquid water, we adopted the PMOw Hamiltonian,[124] which has been specifically parameterized for compounds containing oxygen and hydrogen atoms. Second, a practical and parametrizable procedure is desired to model interfragment electrostatic and exchange-dispersion interactions. Here, for the electrostatic component, we used the dipole preserving and polarization consistent (DPPC) charges to approximate the electrostatic potential of individual fragments. In this approach, the partial atomic charges are derived to exactly reproduce the instantaneous molecular dipole moment from the polarized electron density of each fragment. Since the DPPC charges are optimized by the Langrangian multiplier technique, there are no adjustable parameters. For the ΔE_{XCD} term, we used pairwise Lennard–Jones potentials, which are based two parameters for each atomic number (with pairwise potentials obtained by combining rules). Employing this strategy, we have developed an X-Pol quantum chemical model for water, called the XP3P model, to be used in fluid simulations.

The computed and experimental thermodynamic and dynamic properties of liquid water at 25 °C and 1 atm are listed in Table 2.3, along with the results from an MMFF, namely TIP3P,[8] and from two PMMFFs, namely AMOEBA[39] and SWM4-NDP.[44] The standard errors ($\pm 1\sigma$) were obtained from fluctuations of separate averages over blocks of 2–4 $\times 10^5$ configurations. The average density of XP3P is 0.996 ± 0.001 g/cm^3 which is within 1% of the experimental value

Table 2.3 Computed liquid properties of the XP3P model for water along with those from experiments, and the TIP3P, AMOEBA, and SWM4-NDP models[a]

	XP3P	TIP3P	AMOEBA	SWM4-NDP	Expt.
ΔH_v, kcal/mol	10.42 ± 0.01	10.41	10.48	10.51	10.51
Density, g/cm^3	0.996 ± 0.001	1.002	1.000	1.000	0.997
C_p, cal mol^{-1} K^{-1}	21.8 ± 1.0	20.0	20.9		18.0
$10^6\kappa$, atm^{-1}	25 ± 2	60			46
$10^5\alpha$, K^{-1}	37 ± 3	75			26
μ_{gas}, D	1.88	2.31	1.77	1.85	1.85
μ_{liq}, D	2.524 ± 0.002	2.31	2.78	2.33	2.3-2.6
$10^5 D$, cm^2/s	2.7	5.1	2.02	2.3	2.3
ε	97 ± 8	92	82	79 ± 3	78

[a] ΔH_v, heat of vaporization; C_p, heat capacity; κ, isothermal compressibility; α, coefficient of thermal expansion, μ, dipole moment; D, diffusion constant; and ε, dielectric constant.

and is similar to results obtained with other polarizable and non-polarizable force fields (see Table 2.3). The heat of vaporization was computed using $\Delta H_v = -E_I(I) + RT$, where $E_I(I)$ is the average interaction energy per monomer from the Monte Carlo simulation, and R and T are the gas constant and temperature. The XP3P model for water yielded an average ΔH_v of 10.42 ± 0.01 kcal/mol using the non-variational (charge-embedding) approximation, whereas the value is increased to 10.58 kcal/mol using the variational Fock operator in molecular dynamics. The variational X-Pol approach lowers the interaction energy in the liquid by about 1.5% as compared to the direct charge-embedding approach. Considering the difficulty to achieve converged results on quantities involving fluctuations, including isothermal compressibility, coefficient of thermal expansion and dielectric constant, overall, the agreement with experiment is good, and the performance of the XP3P model is as good as any other empirical force fields in dynamics simulations.

The average molecular dipole moment of molecules in a condensed phase is not well defined, but it is very common for it to be calculated from partial atomic charges or other analysis methods. We calculated the average dipole moment of water in the liquid $< \mu_{liq} >$ to be 2.524 ± 0.002 D, which represents an increase of 35% relative to the gasphase equilibrium-geometry value (1.88 D

from the PMOw Hamiltonian). We found that water molecules in the liquid experience a wide spectrum of instantaneous electrostatic fields from the rest of the system, reflected in the distribution of the instantaneous molecular dipole moments that range from 2.1 to 2.9 D. In MMFF models, the dipole moment is fixed and thus has no fluctuation at all. Of the two PMMFFs in the table, the AMOEBA model produced a much larger dipole moment (2.78 D) than PMOw in the liquid, but the SWM4-NDP model yielded a somewhat small value of 2.46 D. The PMMFF model of Dang and Chang[34] increases the dipole moment from an equilibrium value of 1.81 D in the gas to an average value of 2.75 D in the liquid, and a survey of eight PMMFFs by Chen et al.[35] found average dipole moments in the liquid ranging from 2.31 to 2.83 D. Examining two other PMMFFs, Habershon et al.[147] found average dipole moments of 2.35 and 2.46 D. Stern and Berne,[148] based on a fluctuating charge model type of PMMFF, calculated an equilibrium gas-phase dipole moment of 1.86 D, an average gas-phase dipole moment of 1.92 D (3.6% larger than experiment), and a liquid-phase average dipole moment of 3.01 D. With another PMMFF, Yu and van Gunsteren[42] calculated an equilibrium gas-phase dipole moment of 1.86 D and a liquid-phase average dipole moment of 2.57 D.

Murdachaew et al.[149] used the SCP-NDDO semiempirical molecular orbital model to calculate an increase in the dipole moment from the equilibrium gas-phase value to the liquid-phase value from 2.16 D to 2.8 D, an increase of 30%, whereas with the older PM3[150] and PM6[151] NDDO-type method, which significantly underestimate the polarizability of water, they found that the increase was only 9% and 11%, respectively.

Direct dynamics calculations[152] with the BLYP exchange-correlation functional and electric properties computed from localized Wannier functions predicted an increase of the dipole moment from an equilibrium value of 1.87 D in the gas to an average value of 2.95 D in the liquid.

There is no experimental data for direct comparison, but values ranging from 2.3 to 3.0 D have been advocated, based in part on an estimate for ice Ih.[153,154] The point of these various comparisons of the calculated dipole moment of water in the bulk is not

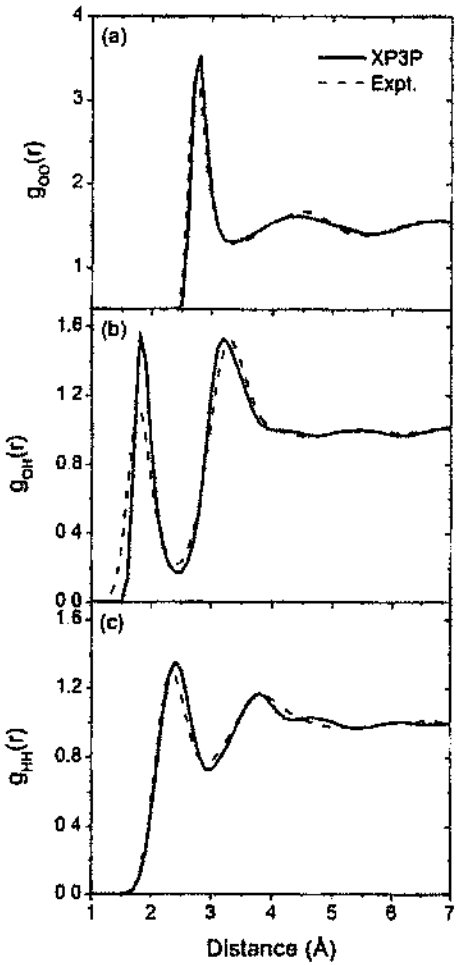

Figure 2.4 Computed (solid) and experimental (dashed) radial distribution functions for O–O, O–H, and H–H pairs in liquid water at 25 °C.

to claim that the X-Pol value is more accurate than the others, but rather to show that it is consistent with the range of previous estimates. Nevertheless, based on analysis of dielectric screening effects of water, Sprik pointed out that an average dipole moment of 2.5–2.6 D in liquid water would most likely yield the correct dielectric constant,[155] and a similar approach was used by Lamoureux et al.[156]

All other thermodynamic and dynamic properties determined using the XP3P model in Table 2.3 are in reasonable accord with experiments and are of similar accuracy in comparison with other empirical models. We note that in contrast to the large number of PMMFFs in the literature that are based on parameterization using different physical approximations, the electronic polarization from the present XP3P model is explicitly described based on a quantum chemical formalism.

Figure 2.4 shows the structure of liquid water characterized by radial distribution functions (RDFs); $g_{xy}(r)$ gives the probability of finding an atom of type y at a distance r from an atom of type x relative to the bulk distribution, where the type is determined by the atomic number. In comparison with the neutron scattering data, the computational results are in excellent agreement with experiments. In particular, a well-resolved minimum following the first peak in the O–O distribution was obtained, whereas the widely used TIP3P and SPC models do not show this feature.[8] For the XP3P potential, the location of the maximum of the first peak of the O-O RDF is 2.78 ± 0.05 Å with a peak height of 3.0. For comparison, the corresponding experimental values are 2.73 Å and 2.8 from neutron diffraction.[157,158] The coordination number of a water molecule in the first solvation layer was estimated to be 4.5, in agreement with the neutron diffraction result of 4.51.[157,158] The oxygen–hydrogen and hydrogen–hydrogen radial distribution functions also agree well with experiments.

2.5 Conclusions

Molecular mechanical force fields (MMFFs) have been successfully used to model condensed-phase and biological systems for a

half century, and more recently polarized molecular mechanics force fields (PMMFFs) have been developed. Thanks to careful parametrization, such classical force fields can be used to provide useful interpretation of experimental findings. In this chapter, we presented a new strategy to construct the potential energy surface for macromolecular systems on the basis of quantum mechanical formalisms. Rather than using quantum chemical results as the target for fitting empirical parameters in the force field, we employ electronic structure theory directly to model intermolecular interactions. As a result, we call this approach a quantum mechanical force field (QMFF).

Our strategy is based on partition of condensed-phase and macromolecular systems into fragments, each of which is explicitly represented by an electronic structure theory with an antisymmetrized wave function. To achieve efficient scaling in the computational cost, the overall molecular wave function of the entire system is approximated by a Hartree product of the individual fragment wave functions. Consequently, the self-consistent field optimization of each molecular wave function can be carried out separately under the influence of the self-consistent polarization by the electric field of the rest of the system. Since the electronic polarization due to interfragment interactions is treated explicitly by electronic structural theory, we call this method the explicit polarization (X-Pol) theory. In this chapter, we summarized the theoretical background of X-Pol and illustrated its application as a versatile electronic structure method to treat intermolecular interactions that can be extended to large molecular and biomolecular systems, including condensed-phase systems. A key application is that we presented an optimized model for statistical mechanical Monte Carlo and molecular dynamics simulations of liquid water by using X-Pol as a QMFF. These illustrative examples in this chapter show that the X-Pol method can be used as a next-generation force field to accurately model molecular complexes and condensed-phase systems and in other work we have also illustrated the method for biomolecular systems.[102]

Acknowledgments

We thank the National Institutes of Health (GM46376) for supporting of this research.

References

1. Hill, T. L. *J. Chem. Phys.* 1946, **14**, 465.
2. Westheimer, F. H. Mayer, J. E. *J. Chem. Phys.* 1946, **14**, 733.
3. Bixon, M. Lifson, S. *Tetrahedron* 1967, **23**, 769.
4. Levitt, M. Lifson, S. *J. Mol. Biol.* 1969, **46**, 269.
5. Levitt, M. *Nat. Struct. Biol.* 2001, **8**, 392.
6. McCammon, J. A. Gelin, B. R. Karplus, M. *Nature* 1977, **267**, 585.
7. Brooks, B. R. Bruccoleri, R. E. Olafson, B. D. States, D. J. Swaminathan, S. Karplus, M. *J. Comput. Chem.* 1983, **4**, 187.
8. Jorgensen, W. L. Chandrasekhar, J. Madura, J. D. Impey, R. W. Klein, M. L. *J. Chem. Phys.* 1983, **79**, 926.
9. Weiner, S. J. Kollman, P. A. Case, D. A. Singh, U. C. Ghio, C. Alagona, G. Profeta, S. Weiner, P. *J. Am. Chem. Soc.* 1984, **106**, 765.
10. Jorgensen, W. L. Tirado-Rives, J. *J. Am. Chem. Soc.* 1988, **110**, 1657.
11. Allinger, N. L. Yuh, Y. H. Lii, J. H. *J. Am. Chem. Soc.* 1989, **111**, 8551.
12. Mayo, S. L. Olafson, B. D. Goddard, W. A. III. *J. Phys. Chem.* 1990, **94**, 8897.
13. Rappé, A. K., Casewit, C. J. Colwell, K. Goddard, W. A. III Skiff, W. *J. Am. Chem. Soc.* 1992, **114**, 10024.
14. Hagler, A. Ewig, C. *Comput. Phys. Commun.* 1994, **84**, 131.
15. Cornell, W. D. Cieplak, P. Bayly, C. I. Gould, I. R. Merz, K. M. Ferguson, D. M. Spellmeyer, D. C. Fox, T. Caldwell, J. W. Kollman, P. A. *J. Am. Chem. Soc.* 1995, **117**, 5179.
16. Halgren, T. A. *J. Comput. Chem.* 1996, **17**, 490.
17. Jorgensen, W. L. Maxwell, D. S. Tirado-Rives, J. *J. Am. Chem. Soc.* 1996, **118**, 11225.
18. MacKerell, A. D. Bashford, D. Bellott Dunbrack, R. L. Evanseck, J. D. Field, M. J. Fischer, S. Gao, J. Guo, H. Ha, S. Joseph-McCarthy, D. Kuchnir, L. Kuczera, K. Lau, F. T. K. Mattos, C. Michnick, S. Ngo, T. Nguyen, D. T. Prodhom, B. Reiher, W. E. Roux, B. Schlenkrich, M. Smith, J. C. State,

R. Straub, J. Watanabe, M. Wiórkiewicz-Kuczera, J. Yin, D. Karplus, M. *J. Phys. Chem. B* 1998, **102**, 3586.

19. Sun, H. *J. Phys. Chem. B* 1998, **102**, 7338.
20. Chen, B. Siepmann, J. I. *J. Phys. Chem. B* 1999, 103, 5370.
21. Cieplak, P. Caldwell, J. Kollman, P. *J. Comput. Chem.* 2001, **22**, 1048.
22. Kaminski, G. A. Friesner, R. A. Tirado-Rives, J. Jorgensen, W. L. *J. Phys. Chem. B* 2001, **105**, 6474.
23. Van Gunsteren, W. F. Daura, X. Mark, A. E. In *Encyclopedia of Computational Chemistry* John Wiley & Sons, Ltd, New York: 2002.
24. Duan, Y. Wu, C. Chowdhury, S. Lee, M. C. Xiong, G. Zhang, W. Yang, R. Cieplak, P. Luo, R. Lee, T. *J. Comput. Chem.* 2003, 24, 1999.
25. Wang, J. Wolf, R. M. Caldwell, J. W. Kollman, P. A. Case, D. A. *J. Comput. Chem.* 2004, **25**, 1157.
26. Oostenbrink, C. Villa, A. Mark, A. E. Van Gunsteren, W. F. *J. Comput. Chem.* 2004, **25**, 1656.
27. Brooks, B. R. Brooks, C. L. Mackerell, A. D. Nilsson, L. Petrella, R. J. Roux, B. Won, Y. Archontis, G. Bartels, C. Boresch, S. Caflisch, A. Caves, L. Cui, Q. Dinner, A. R. Feig, M. Fischer, S. Gao, J. Hodoscek, M. Im, W. Kuczera, K. Lazaridis, T. Ma, J. Ovchinnikov, V. Paci, E. Pastor, R. W. Post, C. B. Pu, J. Z. Schaefer, M. Tidor, B. Venable, R. M. Woodcock, H. L. Wu, X. Yang, W. York, D. M. Karplus, M. *J. Comput. Chem.* 2009, **30**, 1545.
28. Mackerell, A. D. *J. Comput. Chem.* 2004, **25**, 1584.
29. Dykstra, C. E. *J. Am. Chem. Soc.* 1989, **111**, 6168.
30. Bernardo, D. N. Ding, Y. Krogh-Jespersen, K. Levy, R. M. *J. Phys. Chem.* 1994, **98**, 4180.
31. Gao, J. Habibollazadeh, D. Shao, L. *J. Phys. Chem.* 1995, **99**, 16460.
32. Gao, J. Pavelites, J. J. Habibollazadeh, D. *J. Phys. Chem.* 1996, **100**, 2689.
33. Gao, J. *J. Comput. Chem.* 1997, **18**, 1061.
34. Dang, L. X. Chang, T.-M. *J. Chem. Phys.* 1997, **106**, 8149.
35. Chen, B. Xing, J. Siepmann, J. I. *J. Phys. Chem. B* 2000, **104**, 2391.
36. Saint-Martin, H. Hernández-Cobos, J. Bernal-Uruchurtu, M. I. Ortega-Blake, I. Berendsen, H. J. *J. Chem. Phys.* 2000, **113**, 10899.
37. Ren, P. Ponder, J. W. *J. Comput. Chem.* 2002, **23**, 1497.
38. Kaminski, G. A. Stern, H. A. Berne, B. J. Friesner, R. A. Cao, Y. X. Murphy, R. B. Zhou, R. Halgren, T. A. *J. Comput. Chem.* 2002, **23**, 1515.
39. Ren, P. Ponder, J. W. *J. Phys. Chem. B* 2003, **107**, 5933.
40. Kaminski, G. A. Stern, H. A. Berne, B. J. Friesner, R. A. *J. Phys. Chem. A* 2004, **108**, 621.

41. Patel, S. Mackerell, A. D. Brooks, C. L. *J. Comput. Chem.* 2004, **25**, 1504.
42. Yu, H. Van Gunsteren, W. F. *J. Chem. Phys.* 2004, **121**, 9549.
43. Wick, C. D. Stubbs, J. M. Rai, N. Siepmann, J. I. *J. Phys. Chem. B* 2005, **109**, 18974.
44. Lamoureux, G. Harder, E. Vorobyov, I. V. Roux, B. MacKerell, A. D. *Chem. Phys. Lett.* 2006, **418**, 245.
45. Gresh, N. Cisneros, G. A. Darden, T. A. Piquemal, J.-P. *J. Chem. Theory Comput.* 2007, **3**, 1960.
46. Xie, W. Pu, J. MacKerell, A. D. Gao, J. *J. Chem. Theory Comput.* 2007, **3**, 1878.
47. Lopes, P. E. Roux, B. MacKerell, A. D. *Theor. Chem. Acc.* 2009, **124**, 11.
48. Borodin, O. *J. Phys. Chem. B* 2009, **113**, 11463.
49. Xie, W. Pu, J. Gao, J. *J. Phys. Chem. A* 2009, **113**, 2109.
50. Shaw, D. E. Maragakis, P. Lindorff-Larsen, K. Piana, S. Dror, R. O. Eastwood, M. P. Bank, J. A. Jumper, J. M. Salmon, J. K. Shan, Y. Wriggers, W. *Science* 2010, **330**, 341.
51. Zhao, G. Perilla, J. R. Yufenyuy, E. L. Meng, X. Chen, B. Ning, J. Ahn, J. Gronenborn, A. M. Schulten, K. Aiken, C. Zhang, P. *Nature* 2013, **497**, 643.
52. Van Duin, A. C. Dasgupta, S. Lorant, F. Goddard, W. A. III. *J. Phys. Chem. A* 2001, **105**, 9396.
53. Brenner, D. W. Shenderova, O. A. Harrison, J. A. Stuart, S. J. NI, B. Sinnott, S. B. *J. Phys.: Condens. Matter* 2002, **14**, 783.
54. Nielson, K. D. van Duin, A. C. Oxgaard, J. Deng, W.-Q. Goddard, W. A. III *J. Phys. Chem. A* 2005, **109**, 493.
55. Zhao, M. Iron, M. A. Staszewski, P. Schultz, N. E. Valero, R. Truhlar, D. G. *J. Chem. Theory Comput.* 2009, **5**, 594.
56. Vesely, F. J. *J.Comput. Phys.* 1977, **24**, 361.
57. Howard, A. E. Singh, U. C. Billeter, M. Kollman, P. A. *J. Am. Chem. Soc.* 1988, **110**, 6984.
58. Pople, J. A. *Rev. Mod. Phys.* 1999, **71**, 1267.
59. Kohn, W. Becke, A. D. Parr, R. G. *J. Phys. Chem.* 1996, **100**, 12974.
60. Yang, W. *Phys. Rev. Lett.* 1991, **66**, 1438.
61. Gadre, S. R. Shirsat, R. N. Limaye, A. C. *J. Phys. Chem.* 1994, **98**, 9165.
62. Stewart, J. J. P. *Int. J. Quantum Chem.*, 1996, **58**, 133.
63. Dixon, S. L. Merz, K. M. *J. Chem. Phys.* 1996, **104**, 6643.
64. Dixon, S. L. Merz, K. M. *J. Chem. Phys.* 1997, **107**, 879.

65. Gao, J. *J. Phys. Chem. B* 1997, **101**, 657.
66. Gao, J. *J. Chem. Phys.* 1998, **109**, 2346.
67. Kitaura, K. Ikeo, E. Asada, T. Nakano, T. Uebayasi, M. *Chem. Phys. Lett.* 1999, **313**, 701.
68. Wierzchowski, S. J. Kofke, D. A. Gao, J. *J. Chem. Phys.* 2003, **119**, 7365.
69. Zhang, D. W. Zhang, J. Z. H. *J. Chem. Phys.* 2003, **119**, 3599.
70. Zhang, D. W. Xiang, Y. Zhang, J. Z. H. *J. Phys. Chem. B* 2003, **107**, 12039.
71. Hirata, S. Valiev, M. Dupuis, M. Xantheas, S. S. Sugiki, S. Sekino, H. *Mol. Phys.* 2005, **103**, 2255.
72. Collins, M. A. Deev, V. A. *J. Chem. Phys.* 2006, **125**
73. Dahlke, E. E. Truhlar, D. G. *J. Chem. Theory Comput.* 2006, **3**, 46.
74. Dahlke, E. E. Truhlar, D. G. *J. Chem. Theory Comput.* 2007, **3**, 1342.
75. Dułak, M. Kamiński, J. W. Wesołowski, T. A. *J. Chem. Theory Comput.* 2007, **3**, 735.
76. Li, W. Li, S. Jiang, Y. *J. Phys. Chem. A* 2007, **111**, 2193.
77. Xie, W. Gao, J. *J. Chem. Theory Comput.* 2007, **3**, 1890.
78. Hratchian, H. P. Parandekar, P. V. Raghavachari, K. Frisch, M. J. Vreven, T. *J. Chem. Phys.* 2008, **128**
79. Reinhardt, P. Piquemal, J.-P. Savin, A. *J. Chem. Theory Comput.* 2008, **4**, 2020.
80. Xie, W. Song, L. Truhlar, D. G. Gao, J. *J. Chem. Phys.* 2008, **128**
81. R?ezac?, J. Salahub, D. R. *J. Chem. Theory Comput.* 2009, **6**, 91.
82. Song, L. Han, J. Lin, Y.-I. Xie, W. Gao, J. *J. Phys. Chem. A* 2009, **113**, 11656.
83. Sode, O. Hirata, S. *J. Phys. Chem. A* 2010, **114**, 8873.
84. Gao, J. Cembran, A. Mo, Y. *J. Chem. Theory Comput.* 2010, **6**, 2402.
85. Gordon, M. S. Fedorov, D. G. Pruitt, S. R. Slipchenko, L. V. *Chem. Rev.* 2011, **112**, 632.
86. Jacobson, L. D. Herbert, J. M. *J. Chem. Phys.* 2011, **134**
87. Tempkin, J. O. B. Leverentz, H. R. Wang, B. Truhlar, D. G. *J. Phys. Chem. Lett.* 2011, **2**, 2141.
88. Mayhall, N. J. Raghavachari, K. *J. Chem. Theory Comput.* 2011, **7**, 1336.
89. Le, H.-A. Tan, H.-J. Ouyang, J. F. Bettens, R. P. *J. Chem. Theory Comput.* 2012, **8**, 469.
90. Wen, S. Nanda, K. Huang, Y. Beran, G. J. *Phys. Chem. Chem. Phys.* 2012, **14**, 7578.
91. Mayhall, N. J. Raghavachari, K. *J. Chem. Theory Comput.* 2012, **8**, 2669.

92. Wang, Y. Sosa, C. P. Cembran, A. Truhlar, D. G. Gao, J. *J. Phys. Chem. B* 2012, **116**, 6781.
93. Richard, R. M. Herbert, J. M. *J. Chem. Phys.* 2012, **137**, 064113.
94. Qi, H. W. Leverentz, H. R. Truhlar, D. G. *J. Phys. Chem. A* 2013, **117**, 4486.
95. Isegawa, M. Wang, B. Truhlar, D. G. *J. Chem. Theory Comput.* 2013, **9**, 1381.
96. Giese, T. J. York, D. M. *J. Chem. Phys.* 2007, **127**
97. Giese, T. J. Chen, H. Dissanayake, T. Giambaşu, G. M. Heldenbrand, H. Huang, M. Kuechler, E. R. Lee, T.-S. Panteva, M. T. Radak, B. K. York, D. M. *J. Chem. Theory Comput.* 2013, **9**, 1417.
98. Cembran, A. Bao, P. Wang, Y. Song, L. Truhlar, D. G. Gao, J. *J. Chem. Theory Comput.* 2010, **6**, 2469.
99. Gao, J. Wang, Y. *J. Chem. Phys.* 2012, **136**
100. Fedorov, D. G. Ishida, T. Kitaura, K. *J. Phys. Chem. A* 2005, **109**, 2638.
101. Hratchian, H. P. Krukau, A. V. Parandekar, P. V. Frisch, M. J. Raghavachari, K. *J. Chem. Phys.* 2011, **135**, 014105.
102. Xie, W. Orozco, M. Truhlar, D. G. Gao, J. *J. Chem. Theory Comput.* 2009, **5**, 459.
103. Löwdin, P. O. *J. Chem. Phys.* 1950, **18**, 365.
104. Mulliken, R. S. *J. Chem. Phys.* 1955, **23**, 1833.
105. Besler, B. H. Merz, K. M. Kollman, P. A. *J. Comput. Chem.* 1990, **11**, 431.
106. Wang, J. Cieplak, P. Kollman, P. A. *J. Comput. Chem.* 2000, **21**, 1049.
107. Leverentz, H. Gao, J. Truhlar, D. *Theor. Chem. Acc.* 2011, **129**, 3.
108. Momany, F. A. *J. Phys. Chem.* 1978, **82**, 592.
109. Cox, S. Williams, D. *J. Comput. Chem.* 1981, **2**, 304.
110. Singh, U. C. Kollman, P. A. *J. Comput. Chem.* 1984, **5**, 129.
111. Chirlian, L. E. Francl, M. M. *J. Comput. Chem.* 1987, **8**, 894.
112. Breneman, C. M. Wiberg, K. B. *J. Comput. Chem.* 1990, **11**, 361.
113. Wang, B. Truhlar, D. G. *J. Chem. Theory Comput.* 2012, **8**, 1989.
114. Storer, J. Giesen, D. Cramer, C. Truhlar, D. *J. Comput. Aided Mol. Des.* 1995, **9**, 87.
115. Marenich, A. V. Jerome, S. V. Cramer, C. J. Truhlar, D. G. *J. Chem. Theory Comput.* 2012, **8**, 527.
116. Zhang, P. Bao, P. Gao, J. *J. Comput. Chem.* 2011, **32**, 2127.
117. Frisch, M. J. Trucks, G. W. Schlegel, H. B. Scuseria, G. E. Robb, M. A. Cheeseman, J. R. Scalmani, G. Barone, V. Mennucci, B. Petersson, G. A.

Nakatsuji, H. Caricato, M. Li, X. Hratchian, H. P. Izmaylov, A. F. Bloino, J. Zheng, G. Sonnenberg, J. L. Hada, M. Ehara, M. Toyota, K. Fukuda, R. Hasegawa, J. Ishida, M. Nakajima, T. Honda, Y. Kitao, O. Nakai, H. Vreven, T. Montgomery, J. A., Jr. Peralta, J. E. Ogliaro, F. Bearpark, M. Heyd, J. J. Brothers, E. Kudin, K. N. Staroverov, V. N. Kobayashi, R. Normand, J. Raghavachari, K. Rendell, A. Burant, J. C. Iyengar, S. S. Tomasi, J. Cossi, M. Rega, N. Millam, N. J. Klene, M. Knox, J. E. Cross, J. B. Bakken, V. Adamo, C. Jaramillo, J. Gomperts, R. Stratmann, R. E. Yazyev, O. Austin, A. J. Cammi, R. Pomelli, C. Ochterski, J. W. Martin, R. L. Morokuma, K. Zakrzewski, V. G. Voth, G. A. Salvador, P. Dannenberg, J. J. Dapprich, S. Daniels, A. D. Farkas, Ö. Foresman, J. B. Ortiz, J. V. Cioslowski, J. Fox, D. J. *Gaussian Development Version* Gaussian Inc. Wallingford, CT, 2013

118. Zhao, Y. Truhlar, D. G. *Theor. Chem. Acc.* 2008, **120**, 215.
119. Lynch, B. J. Zhao, Y. Truhlar, D. G. *J. Phys. Chem. A* 2003, **107**, 1384.
120. Hehre, W. J. Ditchfield, R. Pople, J. A. *J. Chem. Phys.* 1972, **56**, 2257.
121. Phillips, J. C. Braun, R. Wang, W. Gumbart, J. Tajkhorshid, E. Villa, E. Chipot, C. Skeel, R. D. Kalé, L. Schulten, K. *J. Comput. Chem.* 2005, **26**, 1781.
122. Zhang, P. Fiedler, L. Leverentz, H. R. Truhlar, D. G. Gao, J. *J. Chem. Theory Comput.* 2011, **7**, 857.
123. Isegawa, M. Fiedler, L. Leverentz, H. R. Wang, Y. Nachimuthu, S. Gao, J. Truhlar, D. G. *J. Chem. Theory Comput.* 2012, **9**, 33.
124. Han, J. Mazack, M. J. M. Zhang, P. Truhlar, D. G. Gao, J. *J. Chem. Phys.* 2013, **139**, 054503.
125. Andersen, H. C. *J. Chem. Phys.* 1980, **72**, 2384.
126. Koopman, E. A. Lowe, C. P. *J. Chem. Phys.* 2006, **124**
127. Miyamoto, S. Kollman, P. A. *J. Comput. Chem.* 1992, **13**, 952.
128. Gao, J. Han, J. Zhang, P. *MCSOL version 2012xp* 2012
129. Mazack, M., J. M. Gao, J. *X-Pol. version 2013a1* 2013
130. Wang, B. Truhlar, D. G. *J. Chem. Theory Comput.* 2010, **6**, 3330.
131. Mo, Y. Gao, J. Peyerimhoff, S. D. *J. Chem. Phys.* 2000, **112**, 5530.
132. Mo, Y. Bao, P. Gao, J. *Phys. Chem. Chem. Phys.* 2011, **13**, 6760.
133. Pople, J. A. Santry, D. P. Segal, G. A. *J. Chem. Phys.* 1965, **43**, S129.
134. Cui, Q. Elstner, M. Kaxiras, E. Frauenheim, T. Karplus, M. *J. Phys. Chem. B* 2001, **105**, 569.
135. Elstner, M. *Theor. Chem. Acc.* 2006, **116**, 316.
136. Dewar, M. J. S. Thiel, W. *J. Am. Chem. Soc.* 1977, **99**, 4899.

137. Dewar, M. J. S. Thiel, W. *J. Am. Chem. Soc.* 1977, **99**, 4907.
138. Dewar, M. J. S. Thiel, W. *Theor. Chim. Acta* 1977, **46**, 89.
139. Fiedler, L. Gao, J. Truhlar, D. G. *J. Chem. Theory Comput.* 2011, **7**, 852.
140. Tang, K. T. Toennies, J. P. *J. Chem. Phys.* 1984, **80**, 3726.
141. Grimme, S. Antony, J. Ehrlich, S. Krieg, H. *J. Chem. Phys.* 2010, **132**
142. Grimme, S. Ehrlich, S. Goerigk, L. *J. Comput. Chem.* 2011, **32**, 1456.
143. McNamara, J. P. Hillier, I. H. *Phys. Chem. Chem. Phys.* 2007, **9**, 2362.
144. Morgado, C. A. McNamara, J. P. Hillier, I. H. Burton, N. A. Vincent, M. A. *J. Chem. Theory Comput.* 2007, **3**, 1656.
145. McNamara, J. P. Sharma, R. Vincent, M. A. Hillier, I. H. Morgado, C. A. *Phys. Chem. Chem. Phys.* 2008, **10**, 128.
146. Chang, D. T. Schenter, G. K. Garrett, B. C. *J. Chem. Phys.* 2008, **128**, 164111.
147. Habershon, S. Markland, T. E. Manolopoulos, D. E. *J. Chem. Phys.* 2009, **131**, 024501.
148. Stern, H. A. Berne, B. *J. Chem. Phys.* 2001, **115**, 7622.
149. Murdachaew, G. Mundy, C. J. Schenter, G. K. Laino, T. Hutter, J. *J. Phys. Chem. A* 2011, **115**, 6046.
150. Stewart, J. J. P. *J. Comput. Chem.* 1989, **10**, 209.
151. Stewart, J. J. P. *J. Mol. Model.* 2007, **13**, 1173.
152. Silvestrelli, P. L. Parrinello, M. *Phys. Rev. Lett.* 1999, **82**, 3308.
153. Coulson, C. A. Eisenberg, D. *Proc. R. Soc. London Ser. A* 1966, **291**, 445.
154. Caldwell, J. W. Kollman, P. A. *J. Phys. Chem.* 1995, **99**, 6208.
155. Sprik, M. *J. Chem. Phys.* 1991, **95**, 6762.
156. Lamoureux, G. MacKerell, A. D. Roux, B. *J. Chem. Phys.* 2003, **119**, 5185.
157. Soper, A. *Chem. Phys.* 2000, **258**, 121.
158. Head-Gordon, T., Johnson, M. E. *Proc. Natl. Acad. Sci.* 2006, **103**, 7973.